Precise determination of relative and absolute $\beta\beta$-decay rates of ^{128}Te and ^{130}Te

T. Bernatowicz,[1,2,3] J. Brannon,[1,3] R. Brazzle,[1,2] R. Cowsik,[1,2,4] C. Hohenberg,[1,2] and F. Podosek[1,3]
[1]*McDonnell Center For the Space Sciences, Washington University, St. Louis, Missouri 63130*
[2]*Department of Physics, Washington University, St. Louis, Missouri 63130*
[3]*Department of Earth and Planetary Sciences, Washington University, St. Louis, Missouri 63130*
[4]*Tata Institute of Fundamental Research, Bombay-400005, India*
(Received 18 September 1992)

Double beta decay of ^{128}Te has been confirmed and the ratio of half-lives for $\beta\beta$ decay of ^{130}Te and ^{128}Te has been precisely determined as $T^{130}_{1/2}/T^{128}_{1/2}=(3.52\pm0.11)\times10^{-4}$ by ion-counting mass spectrometry of Xe in ancient Te ores, using techniques that reduce interferences due to trapped Xe. We have also detected excesses of ^{126}Xe originating in high energy reactions of cosmic ray muons and their secondaries on Te; such reactions make minor contributions to the measured ^{128}Xe excesses in the Te ores. The Xe measurements, combined with common Pb dating of the ores, yield a ^{130}Te half-life of $(2.7\pm0.1)\times10^{21}$ yr and thus a ^{128}Te half-life of $(7.7\pm0.4)\times10^{24}$ yr, the longest radioactive decay lifetime measured to date. These results give limits on the effective Majorana mass of the neutrino ($<1.1-1.5$ eV) and right-handed currents ($|\langle\eta\rangle|<5.3\times10^{-8}$) comparable to the best obtained from direct neutrinoless $\beta\beta$-decay searches. They also imply new limits on unconventional Majorons not constrained by measurements of the Z^0 decay width.

PACS number(s): 23.40.Bw, 14.60.Gh, 14.80.Gt, 27.60.+j

I. INTRODUCTION

Double beta ($\beta\beta$) decay has long been recognized as providing important constraints on the nature of extensions to the standard model of electroweak interactions, in particular on the issues of neutrino mass and conservation of lepton number [1]. Nuclear $\beta\beta$ decay occurs in even-even nuclei for which the pairing force between like nucleons energetically forbids ordinary single β decay to an adjacent odd-odd isobar. In principle, there are at least three modes in which such decay can take place: a 2ν mode in which two antineutrinos are emitted along with two electrons,

$$(A,Z)\rightarrow(A,Z+2)+2e^-+2\bar{\nu}\ , \tag{1}$$

a neutrinoless (0ν) mode in which no neutrinos are emitted (resulting from the emission of a virtual neutrino from one neutron and its absorption by another),

$$(A,Z)\rightarrow(A,Z+2)+2e^-+0\bar{\nu}\ , \tag{2}$$

and a 0ν mode accompanied by the emission of a Goldstone boson (Majoron) ϕ,

$$(A,Z)\rightarrow(A,Z+2)+2e^-+0\bar{\nu}+\phi\ . \tag{3}$$

In $\beta\beta$ decay the neutrino may either be a Dirac particle ($\nu\neq\bar{\nu}$) or a Majorana particle ($\nu=\bar{\nu}$), where $\bar{\nu}$ denotes the charge-conjugate state or antiparticle. Observation of the decay mode in Eq. (2) would imply that the neutrino is a Majorana particle and that at least one neutrino eigenstate has a nonzero Majorana mass [2].

$\beta\beta$ decay is a second-order weak interaction, and, consequently, it is one of the slowest processes in nature, with half-lives normally in excess of 10^{20} yr. Although the 2ν decay mode of Eq. (1) has been observed in direct-counting experiments for several isotopes, the low decay rates make laboratory observation challenging and in some cases essentially impossible. The geochemical method of observing decay through daughter isotope excesses in natural samples makes use of geological times over which decays can be integrated. However, in order to be observable the daughter product must make a measurable change in the isotopic composition of the daughter element. In practice, the noble gases, which are normally present in extremely low concentrations in terrestrial materials ($<10^{-8}$ ppm for Xe), are the only group of elements sufficiently scarce to make the geochemical detection of $\beta\beta$ decay experimentally feasible. For example, as early as 1949 Inghram and Reynolds [3] were able to successfully use the noble gas Xe to study the $\beta\beta$ decay of Te. At present, the occurrence of $\beta\beta$ decay for the reactions $^{130}\text{Te}\rightarrow{}^{130}\text{Xe}$ and $^{82}\text{Se}\rightarrow{}^{82}\text{Kr}$ have been established beyond reasonable doubt, and half-lives for these decays have been determined to be 10–30 and 1–2, respectively, in units of 10^{20} yr [4]. The disadvantage of the geochemical method is that it does not directly determine the mode by which the $\beta\beta$ decay occurs, but only gives the sum of all decay channels.

In this study, we are concerned with determination of both absolute and relative $\beta\beta$-decay rates for ^{128}Te and ^{130}Te. This particular isotopic system represents a fortuitous combination of two circumstances favorable to the evaluation of neutrino mass limits, one theoretical and the other experimental. The phase-space dependence of the 2ν decay rate of a given nucleus can be represented as a polynomial in T_0 (where T_0 is the total kinetic energy carried off by the leptons) that varies sharply as T_0^7 to T_0^{11}. The 0ν $\beta\beta$ process varies somewhat less rapidly as

$T_0\langle m\rangle^2$ to $T_0^5\langle m\rangle^2$, where $\langle m\rangle$ is the effective Majorana mass of the neutrino [4,5]. This implies that the relative contribution of $0\nu\ \beta\beta$ decay to the ^{128}Te decay ($T_0=0.87$ MeV) is much larger than that for ^{130}Te ($T_0=2.53$ MeV) for values of $\langle m\rangle$ near the current limits of a few eV. The experimental advantage of the Te system is that both of the daughters of the Te $\beta\beta$ decay, ^{128}Xe and ^{130}Xe, are noble gases which can be easily extracted from Te ores. Their ratio, ^{128}Xe/^{130}Xe, is directly proportional to the ratio of decay rates $\Gamma^{128}/\Gamma^{130}$, and can be determined with relatively high precision by noble-gas mass spectrometry, thus eliminating many sources of systematic error.

These advantages provided by the Te system have prompted many groups to study it, and although the decay of ^{130}Te is well established, there has been a long-standing controversy over whether $\beta\beta$ decay of ^{128}Te has actually been observed. Several studies by the University of Missouri at Rolla group [6–8] have led to positive claims, but work on Te from the Colorado Good Hope Mine by the Heidelberg group [9,10] does not support those observations. One major goal of the present study was to resolve this controversy concerning observation of ^{128}Te $\beta\beta$ decay. We have conducted Xe isotopic analyses on several Te ores, some from the same geological locales (and in several cases from the same samples) as in these prior studies, using high-precision noble-gas mass spectrometry combined with sample handling techniques designed to eliminate nonradiogenic isotopic interferences to as large an extent as possible. As we will show, we have confirmed the existence of ^{128}Te $\beta\beta$ decay and determined the likely source of the previous discrepancy.

In this study we are also concerned with improving constraints on the absolute value of the ^{130}Te half-life, which is significantly uncertain despite several past studies. Theoretically predicted ^{130}Te decay rates are generally 1–2 orders of magnitude faster than the geochemically determined rates [11], in contrast to the fairly good agreement between predicted decay rates for ^{82}Se (using a weak-coupling shell-model calculation [12]) and the experimentally determined rates. In a few cases [10], the ^{130}Te half-life has been derived from ores containing both Se and Te where the geochemically determined ^{82}Se half-life agrees with direct counting results, indicating a real suppression in the ^{130}Te decay rate compared with theory. Nonetheless, current best estimates of the ^{130}Te half-life span a factor of 3 (see Sec. III D), and there is at least the possibility that geochemical estimates of the half-life for ^{130}Te are *very* wrong. This uncertainty arises to a significant extent in establishing the geological age of the Te ore. Chronological data for Te ores are generally scarce, and ages are sometimes inferred only from geological context, which sets an upper limit to the ore age. Even in cases where the age has been determined from the Te ore itself, the chronometer used has always involved a noble-gas daughter, some of which might have been lost from the ore by thermal events or else accidentally inherited during the process of ore formation. Our investigations have therefore included exploration of other geochemical systems in Te ores which might provide improved chronological constraints.

II. SAMPLES AND EXPERIMENTAL PROCEDURES

Three samples of native Te were obtained from P. Dunn of the Smithsonian Institution's National Museum of Natural History: from the American Mine (NMNH R177), Sunshine District, Boulder Co., CO; from the Vulcan Mine (NMNH C88), Gunnison Co., CO; and from the Good Hope Mine (NMNH 85138), Vulcan, CO. The Vulcan and Good Hope mines evidently sample the same ore body [13]. The Good Hope sample is from the same locale as that studied by Kirsten *et al.* in 1968 [14] and 1983 [9]. Each sample consisted of massive polycrystalline Te, and quantitative elemental analysis with a scanning electron microscope energy dispersive x-ray spectrometer (EDS) showed that the samples were at least 99.9% pure Te. We obtained from O. K. Manuel samples of altaite (PbTe; 39.0 wt. % Te) from Mattagami Lake, Quebec and krennerite [(Au,Ag)Te_2; 60.0 wt % Te] from Kalgoorlie, Australia; both of these ores have been previously analyzed by Lee, Manuel and Thorpe [8]. From R. Grauch of the U.S. Geological Survey in Denver we also obtained samples of krennerite (58.8 wt % Te) and calaverite ($AuTe_2$; 57.4 wt. % Te) from Cripple Creek, CO. The Cripple Creek samples are known to be relatively young and we did not expect to observe excess ^{128}Xe in them; they are included in this study to help evaluate the decay rate of ^{130}Te. The Te contents of all samples, determined by EDS analyses, are in satisfactory agreement with published values for specimens from these locales [15].

Country rock adhering to samples was removed using a diamond drill, and larger samples were broken into gram-size fragments which were otherwise unprocessed except for dusting with a dry nitrogen jet. Pieces adjacent to those used for noble-gas analysis were saved for thermal ionization mass spectrometry analysis. Numerous studies (e.g., [16]) have shown that crushing of samples in air can introduce into minerals appreciable quantities of atmospheric Xe which cannot be removed even by lengthy subsequent vacuum exposure at moderate temperatures (several hundred °C), so in order to avoid introducing atmospheric Xe contamination no attempt was made to homogenize samples by crushing in air.

The apparatus used for noble-gas extraction is shown in Fig. 1. The sample was loaded into the apparatus, which was evacuated to $<10^{-8}$ torr and baked overnight at 65 °C to remove surface contaminants. This temperature is sufficiently low that quantitative retention of indigenous Xe in the uncrushed samples is ensured. Gas extraction was accomplished by sample crushing *in vacuo* followed by stepwise heating, except in the case of the altaite, calaverite, and Kalgoorlie krennerite, for which insufficient sample was available for crushing. (These samples were simply loaded into a side arm in the gas extraction system and later subjected to stepwise heating analysis.) In the sample crushing protocol, the sample was pulverized *in vacuo* between two polished hardened steel anvils to release Xe which may have been trapped in small vesicles or crystal boundaries at the time of sample formation. The powder thus produced had a very fine

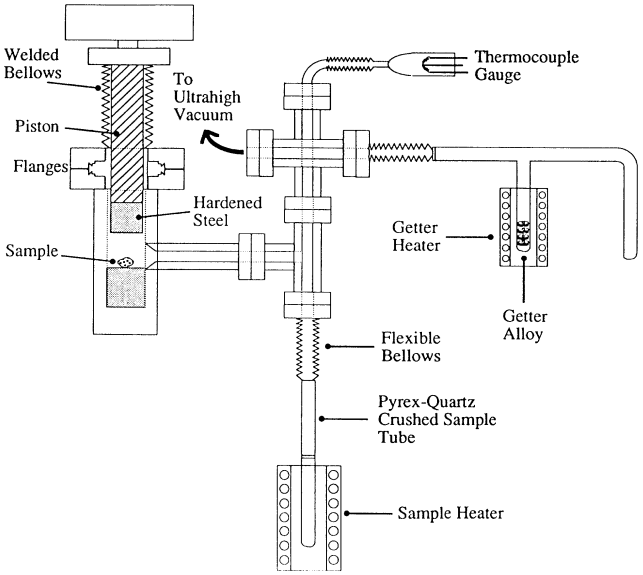

FIG. 1. Schematic of the Xe extraction and gettering apparatus.

grain size, with 99% of the powder in grains less than 20 μm. The Xe released in crushing was analyzed following the procedures described below.

Before the stepwise heating stage, the sample was poured *in vacuo* into a graded seal pyrex-quartz tube which could be externally heated. For the crushed samples, the mass involved in the heating experiments was determined by difference between the original sample mass and that which remained in the crusher at the end of the experiment. It is important to note that the sample transfer procedure was conducted without any intervening exposure of the crushed sample to air, thus avoiding acquisition of atmospheric Xe on the newly created grain surfaces. This protocol was not entirely successful in the case of the Good Hope sample because vibration-induced rupture of a pyrex wall in the extraction apparatus occurred at the start of sample crushing; in this case the crushing was completed after the apparatus was repaired and reevacuated, and the gas released on crushing was analyzed together with gas released from the first heating step at 150 °C. On the basis of subsequently obtained Xe data, this sample appears to have been little contaminated by its brief exposure to air.

Xe was extracted from the sample by stepwise heating in seven or more successively higher 1-h temperature steps, with analysis of Xe following each step, until the Xe levels and isotopic composition approached that of the instrumental background. After the final heating step the native Te samples and altaite had been completely vaporized and recondensed in cooler parts of the extraction tube, ensuring complete Xe extraction. For the krennerite and calaverite samples, a Au residue remained after the bulk of the sample had evaporated. Active gases released by heating were removed by exposure to SAES ST-707 getter alloy held at 400 °C, and progress in the cleanup was monitored with a high vacuum pyrex thermocouple gauge. After initial cleanup, the remaining gases were admitted into the vacuum manifold of the mass spectrometer and exposed to freshly deposited Ti films for further gettering. The Xe was then adsorbed on activated charcoal (at −81 °C, using a mixture of dry ice and acetone) which had been maintained at 150 °C to prevent adsorption of ambient Xe. Ar and other nonadsorbed gases were then pumped away by 10-min exposure to a Hg diffusion pump. The Xe was finally desorbed from the charcoal at 150 °C and admitted to the mass spectrometer for analysis.

The Xe measurements were carried out using a high-sensitivity ion-counting mass spectrometer (21.5 cm, 90° sector) similar to one previously described by Hohenberg [17], which has recently been brought on line in our laboratory and has not been used for any previous analyses except of atmospheric noble gases. This ensures that the Te ore analyses cannot have been affected by spectrometer "memory" effects caused by release of previously implanted anomalous Xe by ion beam scrubbing. Mass discrimination and sensitivity were determined by analysis of known quantities of air Xe. The instrumental mass discrimination at all isotopes was small ($\leq 0.5\%$) and reproducible to better than 0.1% at all isotopes except for the two least abundant ones, ^{124}Xe and ^{126}Xe ($\pm 0.5\%$). The signal strengths for a given quantity of Xe were reproducible to $\pm 2\%$; uncertainties in the absolute abundance of Xe in the present work are less than 5%. Background Xe levels were measured by "blank" runs following the procedures described above except that no sample was used. Blank levels for ^{132}Xe were 10^{-13} cm^3 STP for the crushing step and 5×10^{-15} cm^3 STP for the subsequent heating steps (1 cm^3 STP $= 2.687\times 10^{19}$ atom), and all blanks had atmospheric Xe composition within analytical uncertainties.

For solid element chemical and isotopic analysis, pieces of the Te ores were briefly washed in 1N HCl and 1N HNO_3 to remove surface contamination; these were next crushed to a fine powder, and in the case of the American and Good Hope samples were split in half prior to crushing for replicate analysis. The ore was dissolved in aqua regia, and ion exchange chemistry was performed to isolate elements of potential geochronological interest—K, Ca, Rb, Sr, U, and Pb. Isotopic analyses were performed on a VG-354 thermal ionization mass spectrometer using methods previously described [18]. Absolute elemental abundances were determined by standard isotope dilution techniques.

III. RESULTS

The measured Xe isotopic compositions of each of the Te ores are displayed in Table I. The data have been corrected *only* for instrumental mass discrimination and minor Xe-hydride interferences ($XeH/Xe = 4\times 10^{-4}$); it should be noted that because there is no stable Xe isotope at mass 127 and because the absolute abundance of ^{129}Xe is generally small compared to ^{130}Xe in the Te ores, XeH corrections have an entirely negligible effect on our determination of ^{128}Xe/^{130}Xe from $\beta\beta$ decay. We have not corrected the data in Table I for blanks: the instrumental background Xe is expected and observed to be atmos-

TABLE I. Xe isotopic composition of Te ores. Xe isotopic ratios in Te ores relative to $^{132}Xe = 100.0$. Stated errors in isotopic ratios are 1σ. Data have been corrected only for XeH and instrumental mass discrimination.

Temp.[a] (°C)	^{132}Xe[b] 10^{-15} cm^3/g	Isotopic composition ($^{132}Xe \equiv 100$) ^{124}Xe	^{126}Xe	^{128}Xe	^{129}Xe	^{130}Xe	^{131}Xe	^{134}Xe	^{136}Xe
				American Mine Te (3.9804 g)					
25	253.8	0.3473	0.3535	7.209	105.77	326.2	81.76	39.76	34.09
		±0.0129	±0.0140	±0.067	±0.42	±0.9	±0.28	±0.19	±0.18
200	123.7	0.4042	0.3154	7.341	106.00	340.0	83.62	39.00	33.51
		±0.0212	±0.0216	±0.079	±0.48	±1.4	±0.48	±0.28	±0.24
300	152.3	0.3297	0.3838	8.016	138.48	1971.6	101.06	39.15	32.77
		±0.0192	±0.0215	±0.121	±0.62	±4.8	±0.51	±0.27	±0.27
350	90.8	0.3300	0.4728	9.208	212.56	5746.8	140.72	38.66	32.92
		±0.0239	±0.0216	±0.146	±1.01	±19.9	±0.97	±0.30	±0.31
400	91.9	0.3788	0.4231	9.197	203.60	5291.9	135.32	39.57	33.56
		±0.0277	±0.0274	±0.130	±0.71	±20.1	±0.83	±0.33	±0.25
460	138.9	0.3799	0.3767	8.408	155.53	2896.8	109.64	39.67	33.86
		±0.0209	±0.0195	±0.087	±0.57	±7.6	±0.54	±0.30	±0.20
500	76.0	0.3551	0.3524	8.391	163.82	3367.5	114.68	39.98	34.18
		±0.0320	±0.0364	±0.156	±0.84	±10.3	±0.57	±0.30	±0.25
600	117.6	0.3511	0.3458	7.094	103.80	304.9	80.92	38.70	32.93
		±0.0278	±0.0197	±0.068	±0.46	±1.2	±0.47	±0.31	±0.25
Total	1045.0	0.3581	0.3720	7.923	139.06	2035.7	100.63	39.35	33.52
		±0.0076	±0.0075	±0.036	±0.22	±4.1	±0.19	±0.10	±0.08
				Good Hope Mine Te (2.9988 g)					
150[c]	288.2	0.3536	0.3185	7.148	116.46	132.1	93.30	38.61	32.96
		±0.0211	±0.0165	±0.092	±0.31	±0.3	±0.25	±0.24	±0.22
200	57.1	0.3146	0.3764	7.367	128.44	177.8	99.25	38.83	33.26
		±0.0410	±0.0468	±0.136	±0.98	±1.2	±0.90	±0.36	±0.43
300	151.4	0.3837	0.3265	7.549	288.96	1269.6	225.30	38.77	33.06
		±0.0289	±0.0289	±0.104	±1.23	±5.3	±1.43	±0.31	±0.24
350	122.3	0.3751	0.4110	8.826	759.84	4509.9	608.38	38.78	33.04
		±0.0252	±0.0242	±0.148	±3.05	±17.4	±3.26	±0.36	±0.25
400	158.4	0.3192	0.4592	9.337	1001.05	6221.1	807.21	38.67	33.51
		±0.0296	±0.0300	±0.106	±3.01	±20.8	±2.98	±0.27	±0.20
460	119.3	0.3254	0.3976	8.955	764.27	4520.7	607.59	39.40	33.52
		±0.0289	±0.0417	±0.161	±2.91	±21.4	±3.37	±0.30	±0.31
500	28.3	0.3315	0.3819	7.424	270.35	1194.2	218.27	39.63	33.13
		±0.0616	±0.0702	±0.270	±2.72	±8.5	±2.03	±0.63	±0.51
600	35.6	0.4031	0.3027	7.239	97.69	16.9	77.07	38.22	32.21
		±0.0568	±0.0494	±0.235	±1.13	±0.4	±0.99	±0.59	±0.55
Total	960.6	0.3508	0.3693	8.035	456.45	2447.8	364.73	38.79	33.14
		±0.0110	±0.0110	±0.048	±0.97	±6.4	±0.94	±0.12	±0.10
				Vulcan Mine Te (3.7348 g)					
25	129.8	0.3450	0.3603	7.539	218.90	899.0	177.31	39.07	32.98
		±0.0253	±0.0232	±0.083	±1.02	±2.8	±0.73	±0.28	±0.26
200	56.0	0.3773	0.3436	7.340	200.22	632.2	160.53	38.75	32.56
		±0.0489	±0.0383	±0.173	±1.40	±3.8	±0.86	±0.36	±0.33
250	43.5	0.3663	0.3801	7.717	435.06	2061.1	355.53	39.61	33.18
		±0.0508	±0.0485	±0.166	±2.51	±12.2	±2.41	±0.55	±0.45
300	64.0	0.3724	0.3957	8.539	774.39	4147.5	647.34	40.49	34.42
		±0.0379	±0.0335	±0.148	±4.52	±22.6	±4.16	±0.47	±0.39
350	103.3	0.3225	0.4339	9.137	1076.98	6057.7	919.02	39.93	33.75
		±0.0260	±0.0297	±0.123	±3.91	±22.9	±3.95	±0.25	±0.23
400	52.3	0.3365	0.4892	12.022	2171.14	13078.4	1890.52	39.62	34.01
		±0.0417	±0.0576	±0.232	±8.83	±60.3	±10.36	±0.39	±0.31
460	47.2	0.3650	0.3870	10.646	1535.76	9197.7	1326.09	39.46	34.42
		±0.0436	±0.0492	±0.202	±9.29	±54.6	±9.16	±0.44	±0.45
500	16.3	0.3412	0.3753	10.149	1201.56	7731.1	1080.03	39.04	34.26
		±0.0939	±0.0623	±0.406	±9.62	±58.1	±10.05	±0.86	±0.86

TABLE I. (*Continued*).

Temp.[a] (°C)	^{132}Xe[b] 10^{-15} cm^3/g	Isotopic composition ($^{132}Xe \equiv 100$) ^{124}Xe	^{126}Xe	^{128}Xe	^{129}Xe	^{130}Xe	^{131}Xe	^{134}Xe	^{136}Xe
600	15.4	0.1600	0.3898	7.466	99.18	20.2	80.21	39.56	33.82
		±0.0992	±0.0998	±0.240	±1.15	±1.0	±1.52	±0.81	±0.56
Total	527.8	0.3445	0.3953	8.767	807.95	4503.5	689.79	39.52	33.57
		±0.0134	±0.0134	±0.054	±2.04	±12.4	±1.99	±0.13	±0.12
		Mattagami altaite (2.3381 g; 0.9121 g Te)							
100	12.7	0.2626	0.1723	6.647	98.62	24.7	78.75	37.76	33.16
		±0.1381	±0.1180	±0.399	±1.50	±0.8	±1.65	±0.85	±0.95
200	109.4	0.3704	0.2843	7.109	99.06	38.6	78.75	38.82	33.32
		±0.0389	±0.0339	±0.137	±0.68	±0.4	±0.65	±0.39	±0.33
300	303.5	0.3574	0.3429	7.252	99.07	63.8	79.10	38.51	32.88
		±0.0209	±0.0181	±0.106	±0.37	±0.3	±0.37	±0.25	±0.24
400	154.0	0.3935	0.3154	7.236	101.25	200.1	80.25	39.17	32.97
		±0.0277	±0.0290	±0.156	±0.71	±0.7	±0.48	±0.39	±0.28
450	135.1	0.3320	0.2921	7.408	102.79	327.4	79.66	38.85	32.69
		±0.0311	±0.0316	±0.121	±0.55	±1.4	±0.52	±0.40	±0.30
500	107.5	0.3455	0.3297	7.429	108.40	673.8	82.39	38.85	32.91
		±0.0368	±0.0321	±0.130	±0.90	±3.9	±0.73	±0.43	±0.30
550	106.1	0.4222	0.3896	7.544	113.36	1012.5	85.85	39.07	33.96
		±0.0395	±0.0366	±0.150	±0.69	±4.6	±0.77	±0.35	±0.37
600	122.1	0.4030	0.3255	7.548	110.30	913.5	83.33	38.71	33.06
		±0.0296	±0.0365	±0.119	±0.65	±3.4	±0.56	±0.31	±0.35
650	83.1	0.3587	0.3985	7.869	115.86	1271.8	86.09	39.25	32.26
		±0.0465	±0.0407	±0.162	±1.05	±7.6	±0.71	±0.45	±0.38
700	148.2	0.3131	0.3258	7.850	124.91	1898.5	89.81	38.69	33.27
		±0.0350	±0.0285	±0.097	±0.83	±7.1	±0.48	±0.32	±0.30
750	187.2	0.3451	0.3061	8.244	136.82	2723.8	94.99	38.81	33.27
		±0.0243	±0.0208	±0.104	±0.55	±8.2	±0.38	±0.30	±0.28
800	194.8	0.3410	0.3942	7.799	123.48	1761.2	90.04	39.33	33.77
		±0.0310	±0.0283	±0.112	±0.59	±5.7	±0.54	±0.27	±0.28
850	105.1	0.3481	0.2907	7.435	105.79	523.7	81.95	38.39	32.96
		±0.0249	±0.0305	±0.148	±0.76	±2.5	±0.61	±0.38	±0.34
900	37.5	0.4164	0.4871	7.041	100.60	125.0	80.44	41.06	35.11
		±0.0745	±0.0679	±0.245	±1.13	±1.1	±0.96	±0.72	±0.66
Total	1806.3	0.3589	0.3356	7.543	111.54	935.7	84.32	38.89	33.17
		±0.0089	±0.0083	±0.037	±0.19	±1.7	±0.15	±0.10	±0.09
		Kalgoorlie krennerite (1.1408 g; 0.6839 g Te)							
100	10.0	0.0286	−0.1892	6.621	98.62	121.4	81.88	38.03	32.89
		±0.3576	±0.3291	±0.557	±2.67	±2.5	±2.58	±2.07	±1.66
200	109.7	0.3630	0.3281	7.126	98.38	24.2	78.54	37.94	32.97
		±0.0847	±0.0613	±0.299	±0.99	±0.3	±0.88	±0.62	±0.63
300	473.9	0.3390	0.3390	7.064	99.37	66.7	78.25	38.02	32.58
		±0.0262	±0.0252	±0.133	±0.51	±0.4	±0.42	±0.37	±0.25
350	316.7	0.3713	0.3689	7.220	108.32	546.5	81.87	38.74	32.97
		±0.0329	±0.0319	±0.116	±0.62	±2.8	±0.52	±0.38	±0.40
400	293.6	0.3332	0.3585	10.711	261.72	10006.5	139.30	38.91	32.96
		±0.0307	±0.0331	±0.141	±1.24	±40.0	±0.91	±0.37	±0.30
450	92.7	0.3099	0.3356	16.143	537.11	26857.3	246.03	38.51	32.99
		±0.0660	±0.0646	±0.268	±3.23	±127.8	±1.72	±0.70	±0.58
500	4.5	2.1105	0.3287	7.802	108.24	354.3	83.76	38.53	36.29
		±0.6442	±0.6532	±1.069	±3.55	±8.5	±3.86	±2.62	±1.83
550	4.8	−0.2610	−0.2502	7.638	95.12	173.6	80.73	40.04	33.01
		±0.5916	±0.4012	±0.865	±3.32	±4.5	±2.92	±1.79	±1.66
Total	1305.9	0.3469	0.3432	8.573	169.04	4317.8	104.84	38.43	32.84
		±0.0169	±0.0159	±0.072	±0.50	±19.2	±0.33	±0.20	±0.16

TABLE I. (*Continued*).

Temp.[a] (°C)	^{132}Xe[b] 10^{-15} cm^3/g	Isotopic composition ($^{132}Xe \equiv 100$) ^{124}Xe	^{126}Xe	^{128}Xe	^{129}Xe	^{130}Xe	^{131}Xe	^{134}Xe	^{136}Xe
				Cripple Creek krennerite (3.2033 g; 1.8823 g Te)					
25[f]	185.2	0.3575	0.3326	6.932	98.43	15.3	78.51	38.82	33.00
		±0.0257	±0.0257	±0.088	±0.53	±0.2	±0.42	±0.28	±0.24
25[f]	974.4	0.3302	0.3058	7.121	98.44	15.5	79.09	38.90	33.09
		±0.0099	±0.0097	±0.047	±0.26	±0.1	±0.20	±0.09	±0.14
100	21.8	0.2897	0.1957	6.849	98.29	16.7	78.61	39.61	33.74
		±0.0812	±0.1082	±0.268	±0.82	±0.5	±1.24	±0.69	±0.61
200	108.5	0.3742	0.3164	7.312	99.03	17.4	79.17	38.85	33.01
		±0.0328	±0.0344	±0.145	±0.71	±0.2	±0.63	±0.34	±0.32
300	130.2	0.3787	0.3323	7.265	103.57	28.4	83.81	39.21	33.94
		±0.0316	±0.0310	±0.125	±0.55	±0.2	±0.68	±0.28	±0.31
350	146.1	0.2950	0.2829	7.089	139.28	142.3	124.78	42.05	37.50
		±0.0264	±0.0290	±0.130	±0.58	±0.7	±0.59	±0.39	±0.31
400	69.4	0.2247	0.3909	6.490	331.96	714.6	333.53	48.80	47.15
		±0.0569	±0.0394	±0.164	±1.91	±4.3	±2.60	±0.51	±0.49
450	20.8	0.0717	0.3211	6.747	128.24	115.0	112.72	42.63	39.49
		±0.0956	±0.1124	±0.279	±1.41	±1.5	±1.28	±0.87	±0.70
500	7.5	−0.1813	0.1341	6.957	102.30	22.7	81.26	41.75	36.08
		±0.2999	±0.1979	±0.446	±1.97	±1.0	±1.65	±1.21	±1.10
550	19.0	0.3556	0.1372	6.829	97.45	17.0	81.01	40.95	36.48
		±0.1224	±0.1300	±0.346	±1.38	±0.7	±1.33	±0.75	±0.74
600	67.4	0.3329	0.2048	7.116	96.75	15.2	78.12	38.27	33.18
		±0.0631	±0.0510	±0.144	±0.76	±0.3	±0.77	±0.43	±0.42
700	115.6	0.3169	0.3126	7.319	99.47	15.3	78.46	39.30	33.06
		±0.0642	±0.0523	±0.211	±0.91	±0.3	±0.64	±0.44	±0.58
Total	1865.9	0.3263	0.3055	7.098	111.06	53.6	92.73	39.61	34.13
		±0.0087	±0.0082	±0.035	±0.20	±0.3	±0.19	±0.08	±0.10
				Cripple Creek calaverite (0.3564 g; 0.2044 g Te)					
100	58.2	−0.7490	−0.7356	6.704	97.35	15.3	75.67	38.64	33.20
		±0.2470	±0.3139	±0.495	±2.61	±0.7	±2.17	±1.25	±0.94
200	317.1	0.2359	0.2435	7.260	98.37	14.8	78.20	37.64	32.74
		±0.0638	±0.0668	±0.238	±1.18	±0.4	±1.15	±0.59	±0.61
300	557.0	0.3800	0.2946	7.140	97.55	15.2	80.27	38.87	33.21
		±0.0390	±0.0524	±0.153	±0.87	±0.2	±0.78	±0.54	±0.42
400	557.8	0.3109	0.2115	7.158	102.45	22.9	86.55	38.88	33.52
		±0.0661	±0.0877	±0.245	±1.01	±0.5	±1.00	±0.65	±0.49
500	789.0	0.3221	0.3100	7.024	147.30	101.1	163.91	39.44	33.41
		±0.0392	±0.0357	±0.124	±1.03	±0.7	±0.93	±0.48	±0.31
600	149.7	0.0728	0.0410	7.246	98.35	16.0	78.57	38.33	33.89
		±0.0989	±0.1162	±0.382	±1.26	±0.5	±1.21	±0.90	±0.75
700	77.9	0.1374	0.1105	6.765	99.89	15.8	80.89	39.64	33.65
		±0.1815	±0.1940	±0.503	±1.64	±0.8	±1.90	±0.96	±1.16
Total	2506.7	0.2761	0.2297	7.107	114.52	44.0	107.54	38.88	33.34
		±0.0240	±0.0283	±0.086	±0.48	±0.3	±0.46	±0.26	±0.20
Air[d]		0.353	0.329	7.12	98.33	15.12	78.98	38.81	32.99
		±0.002	±0.002	±0.02	±0.01	±0.03	±0.08	±0.08	±0.06
$^{238}U^{e}_{fission}$							12.74	139.83	168.07
							±0.66	±4.48	±4.80

[a]Extraction temperature for stepwise heating. The 25 °C data are for Xe extracted by *in vacuo* crushing.
[b]Xe concentrations in cm^3 STP/g, based on total sample mass. Absolute concentrations have an uncertainty of less than 5%.
[c]Combination of crushing step and 150 °C heating.
[d]Reference [57].
[e]Reference [58].
[f]Sample was crushed in two successive steps.

pheric in composition and thus is treated as part of the trapped component in the data analysis (Sec. III A).

One of the major reasons for performing noble-gas analyses is that the background abundance of noble gases in minerals is very low, whence small quantities of noble-gas nuclides generated by nuclear processes lead to observable changes in isotopic composition. The traditional complementary problem is that there are frequently multiple sources of Xe isotopes, and the Xe components from these sources must be resolved in order to identify the isotopic components of primary interest, e.g., in the present case the $\beta\beta$-decay daughters ^{128}Xe and ^{130}Xe. Inspection of Table I shows that, in comparison with atmospheric Xe, there are generally enormous isotopic excesses at ^{130}Xe, and these cannot plausibly be attributed to sources other than $\beta\beta$ decay of ^{130}Te. In contrast, isotopic enrichments at ^{128}Xe (and the other Xe isotopes) are substantially smaller, and evaluating the possible sources of these enrichments requires exact calculations which decompose the observed mass spectrum into the constituent contributions.

On the basis of prior experience in the analysis of terrestrial minerals, we anticipate that there will be at least two Xe components in addition to that generated by Te $\beta\beta$ decay. One is comprised of Xe initially trapped in the ore at the time of its formation and/or subsequently occluded from atmospheric sources by a variety of mechanisms (hereafter denoted "trapped" Xe). The second is the result of fission of actinide elements. There are also additional Xe components resulting from the transmutation of Te isotopes by various nuclear particle reactions (derived concentrations of several Xe components in the Te ores are presented in Table IV). In this section we give a detailed account of how the decomposition of the measured Xe spectra into their various components was conducted.

A. Trapped and fissiogenic Xe

The trapped component contributes to all nine isotopes of Xe and is expected to be a small contributor to ^{130}Xe but the major contributor to ^{128}Xe in Te ores. Since the isotopic enrichments of ^{128}Xe are small (Table I), estimation of the trapped Xe composition and, in particular, its contribution to this isotope constitutes the major source of analytical uncertainty in the determination of ^{128}Xe due to $\beta\beta$ decay of ^{128}Te. Nonetheless, experience with all kinds of terrestrial samples indicates that trapped Xe can be expected to have the isotopic composition of atmospheric Xe or possibly a mass-fractionated atmospheric composition (mass fractionation is some smooth compositional dependence on difference in isotopic mass owing to some physical process such as diffusional loss). Correlations of isotopic ratios determined from the stepwise heating data (e.g., Figs. 2–4) reveal that the trapped Xe in the Te ores studied here is generally indistinguishable from unfractionated atmospheric Xe. The predominant form of fission Xe is confidently expected to be that from spontaneous fission of ^{238}U, whose composition is well known (Table I). Fission contributes to the heavy Xe isotopes ^{131}Xe, ^{132}Xe, ^{134}Xe, and ^{136}Xe but does not contribute to the light Xe isotopes ^{124}Xe, ^{126}Xe, ^{128}Xe, and ^{130}Xe, because production of these isotopes through β-decay chains is shielded by stable Te isotopes (^{128}Te and ^{130}Te in this context are effectively stable). Mass 129 isobars are sufficiently far off of the heavy fragment peak of the mass yield distribution that ^{129}Xe production in ^{238}U decay is negligibly small compared to yields for heavier Xe isotopes.

The only known contributions to the three heaviest Xe isotopes (^{132}Xe, ^{134}Xe, and ^{136}Xe) are from the trapped and fission Xe (Table I), and we can use the ratios of these isotopes to resolve these two components. As shown qualitatively in Fig. 2, the individual Xe extraction data for the heavy Xe isotopes are indeed consistent with a mixture of atmospheric and fission Xe. For most of these data, the fission component makes only a small contribution to ^{132}Xe (generally $\leq 1\%$). Because only one isotopic ratio (e.g., ^{136}Xe/^{132}Xe) is necessary to evaluate the relative proportions of the fission and trapped components, and two are available, this is an overdetermined algebraic system. To resolve the two components quantitatively, we used a least-squares algorithm [19] for the ^{132}Xe-^{134}Xe-^{136}Xe system which takes correlated errors into account.

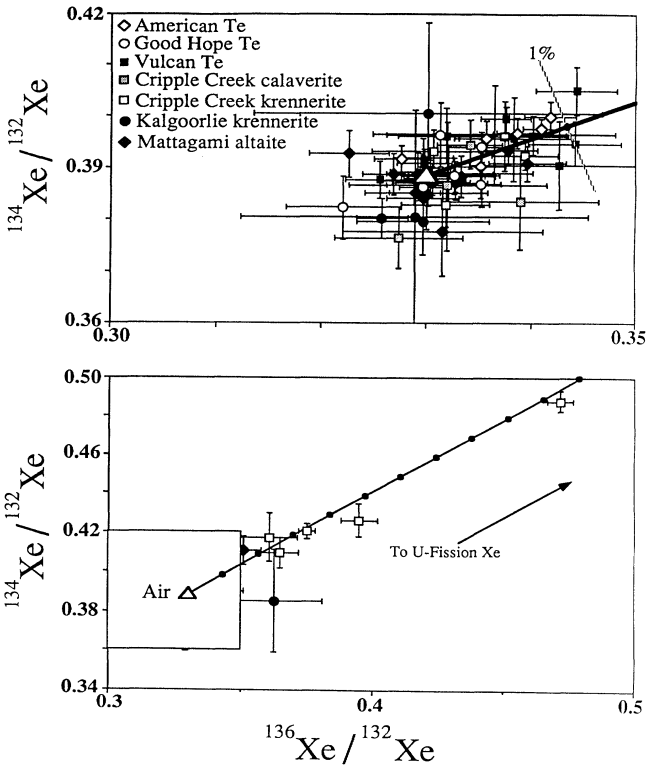

FIG. 2. Three-isotope correlation diagram of heavy Xe isotopes released in vacuum crushing and stepwise heating of Te ores, showing that these isotopes represent a two-component mixture of trapped atmospheric Xe and Xe from spontaneous fission of ^{238}U (cf. Table I). The line in the lower part of the diagram is for a mixture of these two components; the small dots on the line are 1% increments in the fraction of either component contributing to ^{132}Xe. The upper diagram is an enlargement of the boxed area in the lower diagram.

Once the relative proportions of atmospheric and fission Xe are determined from the heavy Xe isotope ratios, these two components are subtracted from the measured isotopic spectrum at all isotopes to which they contribute. The residual or excess Xe isotopic spectra are shown in Table II, with the sample data renormalized to the dominant remaining isotope ^{130}Xe and summed over all Xe extraction steps. As discussed in detail below, these residuals result predominantly from nuclear transmutations (spontaneous and induced) of isotopes of Te.

Since the ^{132}X-^{134}Xe-^{136}Xe system is overconstrained it also provides a consistency check: With our isotopic resolution algorithm the residual abundance of ^{132}Xe necessarily vanishes and the weighted mean abundances of ^{134}Xe and ^{136}Xe must also vanish, but their individual abundances need not. Within errors, however, they do vanish (Table II), indicating that the abundances of these three isotopes can be *quantitatively* understood in terms of a superposition of trapped and fissiogenic components.

Moreover, after the subtraction of the trapped and fissiogenic components, the abundance of ^{124}Xe becomes vanishingly small in most samples. This indicates that source of this isotope is the trapped component alone, and further that the trapped component is atmospheric in composition without any mass fractionation. This means that a high degree of confidence can also be placed in the trapped Xe corrections to ^{128}Xe and ^{130}Xe and the resulting determination of the radiogenic ^{128}Xe/^{130}Xe ratio (Table II). In the case of the Cripple Creek samples, there does appear to be some fractionation of the trapped Xe, as is evident from the nonvanishing ^{124}Xe residuals (Table II). Because they are too young (Table VI), these samples are not used in determining the radiogenic ^{128}Xe/^{130}Xe ratio, and slight mass fractionation of the Xe does not compromise our ability to resolve trapped ^{130}Xe from the measured abundance of this isotope.

Even the very small quantities of fission Xe derived for our native Te samples are in several instances too large to be accounted for by the measured U concentrations (≤ 3 ppb; Table IV) during the lifetimes of these ores. Although the Good Hope fission Xe gives a formation age roughly consistent with the geological age of the ore deposit (Sec. III D), the inferred U-fission Xe ages for the American Mine and Vulcan Mine are in excess of the age of the earth. We thus infer that for the latter samples some of the fission Xe must have been inherited by the ores during their formation. This is not unreasonable, since the hydrothermal fluids from which the Te was deposited may have traversed granitic rocks comparatively rich in actinides and scavenged fission Xe from them. The Cripple Creek krennerite, on the other hand, has a far greater U concentration (~ 2 ppm) so is fairly insensitive to inherited fission Xe of the levels in the native Te samples; it gives a U-Xe age of $(23\pm 2)\times 10^6$ yr, roughly consistent with a geological age of 28×10^6 yr for the Cripple Creek Te ores [20].

B. Xe from neutron capture on Te

Inspection of the residual Xe isotopic spectrum (Table II) reveals that there are significant excesses of ^{129}Xe and ^{131}Xe. These may plausibly be attributed to neutron capture on ^{128}Te and ^{130}Te, respectively, as has been noted in previous studies of Te ores [3,6,21,22]. In the case of the Te ores in this study, both ^{129}Xe and ^{131}Xe released in

TABLE II. Isotopic compositions of Te-derived Xe. Isotopic composition from Table I, with initial trapped atmospheric Xe and fissiogenic Xe removed (cf. footnotes d and e, Table I). Data are isotopic ratios relative to ^{130}Xe$\equiv$100. Stated errors are 1σ. ^{132}Xe was used as the reference isotope in the trapped-fission Xe decomposition, so its residual abundance is nil.

Sample	^{130}Xe[a] (10^{-12} cm^3 STP/g)	Isotopic Composition (^{130}Xe$\equiv$100; ^{132}Xe$\equiv$0) ^{124}Xe	^{126}Xe	^{128}Xe	^{129}Xe	^{131}Xe	^{134}Xe	^{136}Xe
American Mine native Te	21.20	0.000 33 ±0.000 38	0.002 20 ±0.000 37	0.041 3 ±0.001 9	2.04 ±0.02	1.086 ±0.012	0.005 ±0.007	−0.003 ±0.007
Good Hope Mine native Te	23.37	−0.000 08 ±0.000 46	0.001 67 ±0.000 46	0.037 8 ±0.002 2	14.72 ±0.05	11.749 ±0.044	−0.004 ±0.008	0.002 ±0.007
Vulcan Mine native Te	23.77	−0.000 15 ±0.000 30	0.001 52 ±0.000 30	0.037 5 ±0.001 3	15.82 ±0.05	13.616 ±0.049	0.004 ±0.005	−0.002 ±0.005
Mattagami altaite	42.62	0.000 69 ±0.000 97	0.000 76 ±0.000 90	0.046 7 ±0.004 4	1.45 ±0.03	0.587 ±0.026	−0.003 ±0.017	0.004 ±0.016
Kalgoorlie krennerite	93.73	−0.000 14 ±0.000 40	0.000 33 ±0.000 38	0.033 8 ±0.001 17	1.64 ±0.01	0.601 ±0.008	−0.009 ±0.005	−0.004 ±0.004
Cripple Creek krennerite	1.227	−0.063 3 ±0.027 4	−0.055 5 ±0.050 8	0.095 ±0.127	35.09 ±0.90	37.04 ±0.65	−0.104 ±0.333	0.043 ±0.365
Cripple Creek calaverite	1.265	−0.259 1 ±0.085 9	−0.336 8 ±0.101 3	0.090 ±0.355	57.79 ±3.23	100.05 ±2.89	−0.272 ±1.363	0.315 ±1.113

[a]Absolute ^{130}Xe concentration normalized to Te mass only. Uncertainty is $\leq 5\%$.

stepwise heating correlate with the radiogenic ^{130}Xe produced from $\beta\beta$ decay of ^{130}Te. This is illustrated in Fig. 3, where we plot the ^{129}Xe/^{132}Xe and ^{131}Xe/^{132}Xe ratios as a function of ^{130}Xe/^{132}Xe. The data describe a mixing relationship between atmospheric Xe and a Te-derived component, with the composition of the latter differing among samples because of the differences in their neutron exposures. Since ^{132}Xe is not radiogenic (the data have been corrected for small amounts of fission Xe, as described above), the point corresponding to the component derived from Te lies at infinity, and the slopes of the various correlation lines give the ratio of ^{129}Xe and ^{131}Xe from neutron capture to ^{130}Xe from $\beta\beta$ decay. The fact that these correlation lines pass through the point corresponding to atmospheric Xe within analytical uncertainty again indicates that the trapped Xe in the native Te samples is compositionally identical to atmospheric Xe.

The ratio of excess ^{129}Xe to ^{131}Xe varies among the samples studied here (from 0.6 to 2.7; Table III), and is in most cases markedly greater than the ratio of approximately 0.6 expected from thermal neutron capture on ^{128}Te and ^{130}Te. Browne and Berman [23] have shown that resonance capture of epithermal neutrons can produce ^{129}Xe/^{131}Xe ratios up to 4, so it is likely that much of the variability of this ratio in our samples comes from differences in the proportions of thermal and resonance

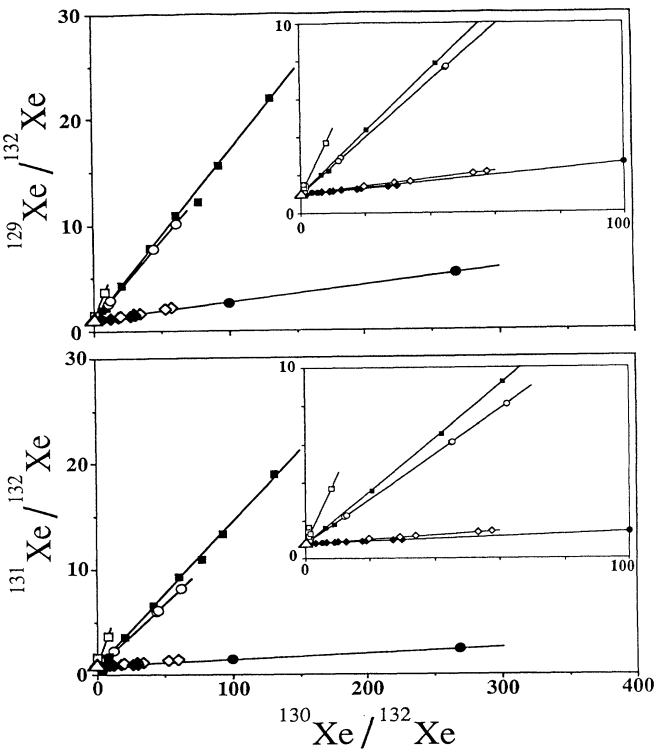

FIG. 3. Correlations of ^{129}Xe and ^{131}Xe from (n,γ) reactions on Te with ^{130}Xe from $\beta\beta$ decay of ^{130}Te. Symbols have same meaning as in Fig. 2. Error bars are smaller than the symbols. The correlations for various extractions from a given sample indicate that the ^{129}Xe and ^{131}Xe excesses, like those of ^{130}Xe, are derived from Te; the variable correlation slopes for the different samples reflect different neutron exposure conditions. See text for discussion.

neutrons captured by the various ores. Using the neutron capture cross sections for both types of reaction [23,24] in conjunction with the excess ^{129}Xe/^{131}Xe ratio permits a determination of the integrated neutron exposure for each sample as well as the thermal and resonance neutron fractions. The excess ^{129}Xe/^{131}Xe ratio sets only an upper limit on the thermal neutron fraction and a lower limit on the ratio of integrated neutron cross sections, because the ^{129}I generated by neutron capture on ^{128}Te in the last mean lifetime of ^{129}I (23×10^6 yr) will not have yet decayed to ^{129}Xe. The results of these calculations are displayed in Table III. The fluences vary by an order of magnitude among samples, an important conclusion that we will return to in our discussion of the observed ^{128}Xe excesses.

We cannot unambiguously determine the source of the neutrons, but it is clear that for all ores except the Cripple Creek krennerite, they cannot have come largely from (α,n) reactions or ^{238}U fission in the ores themselves since the abundance of ^{238}U (Table IV) falls at least a factor of several (American Mine and Cripple Creek calaverite samples) to 2 orders of magnitude short (Good Hope Mine sample) of accounting for them. The mean free path for neutron capture in rock is of the order 1–2 m, however, so the neutrons could originate in rocks surrounding the ores if their U concentrations were at least a few tens to a few hundreds of ppb. This is entirely reasonable for average terrestrial crustal rocks whose U concentrations are typically 1–2 orders of magnitude greater than these values. However, it requires the Te ores to have captured up to 10% or so of the available neutrons, which may or may not be reasonable depending upon the concentration of Te ore in the host rock and how strongly the host rock competes for neutrons. A possible additional source of neutrons is high energy reactions of cosmic ray muons with subterranean target nuclides (Sec. III C 5). In the case of the Cripple Creek krennerite, the number of neutrons produced in the ore is twice the number of atoms of ^{129}Xe and ^{131}Xe resulting from neutron capture, so that ^{238}U decay in the ore itself could account for at least a minor portion of these isotopes. We note that, in all cases, the neutron fluences are far too low to produce significant fission Xe from ^{235}U: for the fluences in Table III, Xe from ^{235}U neutron-induced fission will be at least 5 orders of magnitude less abundant than that from spontaneous fission of ^{238}U.

C. ^{128}Xe excesses

Subtraction of the trapped Xe contribution to ^{128}Xe reveals significant excesses of this isotope for all of the Te ores except the young samples from Cripple Creek, which have large errors because of the relatively low ratio of Te-derived Xe to trapped Xe. There are excesses in the total isotopic compositions (displayed in Table II) as well as in individual stepwise heating analyses; note that the excesses of ^{128}Xe are strictly correlated with excesses of ^{130}Xe due to $\beta\beta$ decay of ^{130}Te. An example of this correlation is shown in Fig. 4, a plot of all of the Table I data for the native Te ores. The fact that ^{128}Xe/^{132}Xe ratios in the data are often appreciably in excess of the atmospher-

TABLE III. Neutron capture production of Xe isotopes in Te ores. Isotopic ratios and abundances resulting from n-capture reactions on ^{128}Te and ^{130}Te, calculated from Table II data.

Sample	$^{129}Xe_{nc}$ (10^{-12} cm^3 STP/g)[a]	$^{131}Xe_{nc}$ cm^3 STP/g)[a]	$(^{129}Xe/^{131}Xe)_{nc}$[b]	Total neutron fluence[c] (10^{10} n/cm^2)	Thermal neutron fraction[d]	$\sigma_{128}/\sigma_{130}$[d,e]
American Mine native Te	0.431	0.229	1.876 ±0.021	1.66	≤0.66	≥2.00
Good Hope Mine native Te	3.44	2.74	1.253 ±0.006	20.5	≤0.83	≥1.34
Vulcan Mine native Te	3.74	3.22	1.162 ±0.005	24.1	≤0.86	≥1.24
Mattagami altaite	0.618	0.250	2.463 ±0.120	1.76	≤0.49	≥2.63
Kalgoorlie krennerite	1.54	0.563	2.734 ±0.040	3.92	≤0.41	≥2.91
Cripple Creek krennerite	0.431	0.454	0.947 ±0.029	3.43	≤0.91	≥1.01
Cripple Creek calaverite	0.731	1.27	0.578 ±0.036	9.71	≤1.0	≥0.62

[a]Concentrations are per gram of Te.
[b]Predicted Xe production ratios are 0.62 for thermal capture [24] and 4.0 for epithermal resonance capture [23].
[c]Assuming thermal neutron cross sections of 0.145 b and 0.22 b [24] and resonance capture cross sections of 1.098 b and 0.258 b [23] for ^{128}Te and ^{130}Te, respectively.
[d]Values stated as limits because ^{129}I produced by neutron exposure of ^{128}Te in its last mean lifetime (23×10^6 yr) has not yet decayed to ^{129}Xe.
[e]Ratio of total n-capture cross sections.

TABLE IV. Xe component and trace element concentrations in Te ores. Absolute concentrations of trapped and fissiogenic Xe are based on total sample weight; concentrations for radiogenic ^{130}Xe and nucleogenic ^{131}Xe are based on Te mass only. Uncertainty in concentrations is ≤5%.

Sample	Initial[a] trapped ^{132}Xe	Fissiogenic[b] ^{136}Xe	Radiogenic[c] ^{130}Xe	Nucleogenic[d] ^{131}Xe	[U][e] (ppb)	[Pb][e] (ppm)
		(10^{-12} cm^3 STP/g)				
American Mine native Te	1.04	0.0082 ±0.0009	21.20	0.229	0.9	0.55
Good Hope Mine native Te	0.960	0.0018 ±0.0009	23.37	2.74	3.0	2.7
Vulcan Mine native Te	0.525	0.0049 ±0.0007	23.77	3.22	0.8	0.8
Mattagami altaite	1.80	0.0038 ±0.0012	42.62	0.250		(61%)[f]
Kalgoorlie krennerite	1.31	≤0.0011	93.73	0.563		
Cripple Creek krennerite	1.85	0.0254 ±0.0015	1.227	0.454	2200	
Cripple Creek calaverite	2.50	0.0108 ±0.0052	1.265	1.27		

[a]Trapped atmospheric Xe. For relative concentration of other atmospheric Xe isotopes, cf. footnote d, Table I.
[b]Xe from spontaneous fission of ^{238}U. For relative concentrations of other fissiogenic Xe isotopes, cf. footnote e, Table I. Stated error limits (1σ) are those resulting from uncertainties in isotopic ratios used in the fission Xe-trapped Xe decomposition. Concentrations have an additional 5% uncertainty from variations in absolute instrumental sensitivity (caption).
[c]From $\beta\beta$ decay of ^{130}Te. Relative concentration of ^{128}Xe from $\beta\beta$ decay of ^{128}Te is listed in Table V.
[d]From ^{130}Te(n,γ). For ^{129}Xe from ^{128}Te(n,γ) see Table III.
[e] Determined by solid source mass spectrometry, using isotope dilution techniques.
[f]Pb concentration from energy dispersive x-ray analysis.

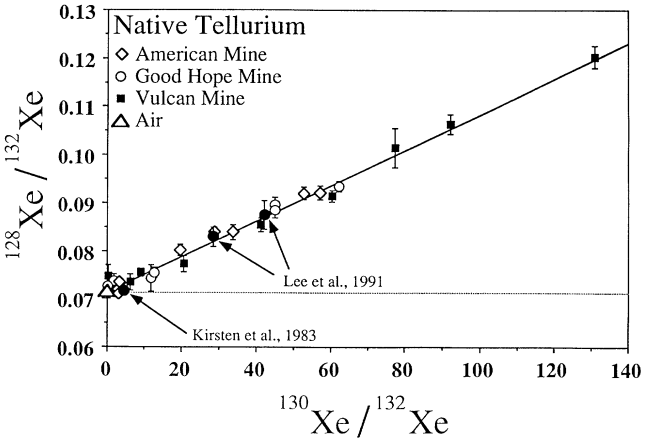

FIG. 4. Correlation of ^{128}Xe with ^{130}Xe for Colorado native Te vacuum crushing and stepwise heating data, representing primarily a mixture of atmospheric Xe and $\beta\beta$-decay Xe. The data (from Table I) show clear excesses of ^{128}Xe that correlate with ^{130}Xe from $\beta\beta$ decay of ^{130}Te. The correlation line is a least-squares fitting to the data. Data from previous work are also shown, but have not been included in the fitting. See text for discussion.

ic value and are correlated with excess ^{130}Xe assures us that radiogenic contributions to ^{128}Xe are definitely observed. Least-squares fitting of these data is consistent with a linear relationship (reduced $\chi^2=0.977$, with the number of degrees of freedom of 22) between $^{128}Xe/^{132}Xe$ and $^{130}Xe/^{132}Xe$, indicative of simple two-component mixing among these three Xe isotopes. One of the components is trapped atmospheric Xe, since the mixing line passes through this composition within analytical uncertainty. The other component, presumably derived from nuclear transmutations of Te, lies along the correlation line at essentially an infinite distance from the atmospheric Xe datum on this diagram, since the atmospheric component contributes virtually all of ^{132}Xe (except for a very small fissiogenic contribution). The slope of the mixing line is essentially equivalent to the mean of the Te-derived $^{128}Xe/^{130}Xe$ ratios for native Te displayed in Table II.

In Fig. 4 we also compare the results of the present experiment with those obtained for altaite and krennerite by Lee, Manuel, and Thorpe [8] and for the Good Hope native Te by Kirsten, Richter, and Jessberger [9]. The two data points from Lee, Manuel, and Thorpe [8] represent the most radiogenic compositions from their stepwise heating data, and these are seen to be entirely consistent with our Te-derived $^{128}Xe/^{130}Xe$ ratio, since they lie on the correlation line defined by our data. Comparison of our results for the Good Hope Mine native Te with that of the most radiogenic composition measured in 1983 by Kirsten, Richter, and Jessberger [9] (at 480 °C, with $^{130}Xe/^{132}Xe=4.2$) shows that their sample is highly enriched in the atmospheric Xe component compared to our sample. Our most radiogenic Good Hope fraction (400 °C; cf. Table I) has a substantially higher $^{130}Xe/^{132}Xe$ ratio of 62, and all but our first two extraction steps have $^{130}Xe/^{132}Xe$ ratios greater than that of the Kirsten-Richter-Jessberger [9] 480 °C datum.

Because of the consistency of our altaite and krennerite results with those of Lee, Manuel and Thorpe [8] and because all of the Good Hope samples should be intrinsically equivalent we cannot easily ascribe the differences between our Good Hope results and those of the Heidelberg group to errors in the noble-gas mass spectrometry, to the data analysis procedure, or to variability of the samples themselves. Indeed, there is no difference between the total radiogenic ^{130}Xe concentration of our Good Hope sample (Table IV) and that in the 1968 analysis of Good Hope native Te by Kirsten *et al.* [14]. We thus consider it likely that their sample processing, which evidently consisted of grinding the sample into fine particles [14], introduced significant quantities of atmospheric Xe into their sample. Our analysis of the 1983 Kirsten-Richter-Jessberger [9] results indicates that their extraction at 480 °C in itself had 4–5 times as much atmospheric ^{132}Xe as that in the *total* Xe extracted from our Good Hope Mine sample (Table IV). Because the abundance of ^{128}Xe in air is roughly half that of the ^{130}Xe abundance and the production of ^{128}Xe in $\beta\beta$ decay is at least several orders of magnitude less than that of ^{130}Xe, atmospheric contamination has a much more important effect at ^{128}Xe than at ^{130}Xe. This is not a complete explanation of the apparent discrepancy, however, because the radiogenic $^{128}Xe/^{130}Xe$ ratios obtained by us are well outside the Kirsten-Richter-Jessberger [9] stated error limits. But it is clear that the large atmospheric component makes resolution of the radiogenic ^{128}Xe sensitively dependent on the details of the Xe component resolution algorithm.

The mean Te-derived $^{128}Xe/^{130}Xe$ ratio for the present set of analyses (Table V), exclusive of the Cripple Creek samples, is $(3.77\pm0.08)\times10^{-4}$, which could be taken as the production ratio in $\beta\beta$ decay of ^{128}Te and ^{130}Te, *provided that no other nuclear reactions contribute to* ^{128}Xe. This point requires explicit attention, because *any* Xe component in the Te ore which is released in constant proportion to the excess ^{130}Xe component will result in an isotopic correlation such as is observed in Fig. 4. Contributions to the large amounts of excess ^{130}Xe other than from $\beta\beta$ decay are demonstrably negligible, so the Te-derived $^{128}Xe/^{130}Xe$ ratio of $(3.77\pm0.08)\times10^{-4}$ is a strict upper limit to the $\beta\beta$-decay production ratio. However, in order to arrive at a definitive production ratio, additional possible nucleogenic contributions to the substantially smaller excess of ^{128}Xe need to be considered. In the following sections we examine these other possible sources of excess ^{128}Xe.

1. $^{127}I(n,\gamma\beta^-)^{128}Xe$ reactions

The most prolific nuclear process which is likely to produce excess ^{128}Xe is $(n,\gamma\beta^-)$ reactions on ^{127}I. By means of reactor irradiation of a gold telluride in which excess ^{128}Xe had been previously observed, Hennecke, Manuel, and Sabu [6] demonstrated that $(n,\gamma\beta^-)$ reactions could not account for the excess ^{128}Xe. From their data we calculate an iodine concentration of several hundred ppb for their sample. Using the neutron fluences given in Table III and a similar iodine concentration, and taking into account both thermal and resonance capture cross sections, we calculate that neutron capture on

iodine could account for at most only a few percent of the observed excesses of ^{128}Xe in our samples.

A more direct evaluation can be made by comparing how the abundance of excess ^{128}Xe varies with neutron fluence. If the excess ^{128}Xe comes predominantly from neutron capture, we would expect the abundance of excess ^{128}Xe to scale with increasing neutron exposure. We can compare the integrated neutron fluence for individual samples (Table III) with the excess ^{128}Xe/^{130}Xe ratios resulting from correction of the data for all other relevant reactions (Table V). The (1σ) dispersion of the corrected ratios is only about 7% of the mean value, despite the fact that the neutron fluences vary among samples by over an order of magnitude. Excepting the very unlikely coincidence that iodine content varies inversely with neutron fluence, we conclude that the observed excess ^{128}Xe cannot result from neutron capture on ^{127}I, although we cannot exclude the possibility of very small ($\sim 1\%$) contributions from this source.

2. α-particle reactions

There are two α-particle reaction channels that can result in the production of ^{128}Xe, namely, ^{124}Te$(\alpha,\gamma)^{128}$Xe and ^{125}Te$(\alpha,n)^{128}$Xe. The requisite α's must come from U and Th decay within the Te ores themselves, since the mean free paths of these particles are far too short (<50 μm for 6–9 MeV α particles) for external sources to contribute. The average U concentrations (and presumably Th concentrations, assuming the typical terrestrial Th/U of 3–4) in our samples are quite low (<3 ppb for the native Te samples, Table IV), and α-particles from these elements are unlikely to be sufficient in producing the excess ^{128}Xe. One can make a quantitative evaluation of this possibility: Haxton [25] estimated the range and energy profiles of the α particles as they move through Te, and using an optical-model estimate of the cross sections, calculated production rates from Te. His results, combined with our measured U concentrations, indicate that α reactions would fall at least 5 orders of magnitude short of accounting for the observed excess ^{128}Xe in our samples.

3. Solar neutrino reactions

The interaction of electron neutrinos with matter is extremely weak, but the Sun emits prodigious quantities of these particles (10^{34}/sec from ^{8}B decay) and the interaction of energetic solar neutrinos with Te is a possible source of Xe. The reaction relevant to the current discussion is the transmutation of ^{128}Te to ^{128}Xe. Bozoki and Lande [26] have calculated the yield for this process in terms of a simulated lifetime for ^{128}Te, which turns out to be an effective half-life of 4×10^{29} yr. This is 4 orders of magnitude longer than the ^{128}Te half-life that would be inferred from the present results and seemingly rules out neutrino reactions as a source of ^{128}Xe.

We have made an independent calculation for the native Te samples based upon their age (about 1.6×10^{9} yr; Sec. III D), and the ^{8}B neutrino flux (5.8×10^{6} cm^{-2} sec^{-1}) and cross section (2.1×10^{-42} cm^{2}) given by Haxton [27]. We find that neutrino interactions could account for $\leq 0.2\%$ of the $\sim 2.5\times10^{5}$ atom/g excess ^{128}Xe in these samples, and thus seem to merit no further consideration.

4. Cosmic ray spallation reactions

Cosmic ray spallation from isotopes of Ba and the rare-earth elements must also be evaluated as a potential source of Xe. Although the flux of most cosmic rays is rapidly attenuated at the Earth's surface, there is at least the possibility that the more penetrating muons may induce spallation reactions resulting in the production of

TABLE V. Relative Te $\beta\beta$-decay Xe production and half-lives. Ratio of $\beta\beta$-decay Xe production of ^{128}Xe and ^{130}Xe and half-lives for ^{130}Te and ^{128}Te, in units of 10^{-4}. Stated uncertainties are 1σ.

Sample	Te-derived[a] ^{128}Xe/^{130}Xe (10^{-4})	Muon corrected[b] ^{128}Xe/^{130}Xe (10^{-4})	Uncorrected[a] $T_{1/2}(130)/T_{1/2}(128)$ (10^{-4})	Muon corrected[b] $T_{1/2}(130)/T_{1/2}(128)$ (10^{-4})
American Mine	4.13	3.37	4.40	3.59
native Te	±0.19	±0.23	±0.20	±0.24
Good Hope Mine	3.78	3.20	4.03	3.41
native Te	±0.22	±0.27	±0.23	±0.29
Vulcan Mine	3.75	3.22	4.00	3.44
native Te	±0.13	±0.17	±0.14	±0.18
Mattagami	4.67	4.41	4.98	4.70
altaite	±0.44	±0.54	±0.47	±0.58
Kalgoorlie	3.38	3.27	3.61	3.48
krennerite	±0.17	±0.22	±0.18	±0.23
Mean value[c]	3.77	3.30	4.02	3.52
	±0.08	±0.10	±0.09	±0.11

[a]Ratio based on Table II Te-derived ^{128}Xe and ^{130}Xe, not corrected for cosmic ray muon production of ^{128}Xe.

[b]Ratio corrected for cosmic ray muon contributions to ^{128}Xe, assuming equal cross sections per nucleon for ^{126}Te and ^{128}Te and using the muon-derived ^{126}Xe excesses given in Table II.

[c]Stated uncertainties are 1σ in mean of all samples listed.

the lighter Xe isotopes [27]. Spallation from Te itself cannot produce Xe, so the targets would have to be minor or trace elements in the Te ores. At least in the case of the native Te samples, the trace element concentrations that have been determined appear to be quite low [28], although we have not measured any of the directly relevant target abundances. Arguing from the opposite direction, we conclude that spallation reactions cannot be significant contributors to ^{128}Xe in our samples ($<1\%$), because spallation yields of ^{124}Xe, ^{126}Xe, and ^{128}Xe are roughly comparable, whereas the observed excesses of ^{126}Xe and especially ^{124}Xe (as noted above in Sec. III A) in our samples are much smaller than those of ^{128}Xe.

5. *Muon and (p,n) reactions, excess ^{126}Xe and ^{128}Xe*

Another source of ^{128}Xe that we must consider is (p,n) reactions on ^{128}Te. Although the flux of cosmic ray protons is sufficiently high (of order 10^{-3} cm^{-2} sec^{-1}) at the Earth's surface to conceivably generate non-negligible levels of ^{128}Xe by ^{128}Te(p,n) reactions, the proton flux rapidly diminishes in rock (with an absorption e-folding depth of about $\frac{1}{2}$ m). Near-surface proton interactions cannot account for the *bulk* of the ^{128}Xe excesses in the Te ores studied, however, because the Kalgoorlie krennerite was taken from a well-documented depth of about 300 m [29], and its excess ^{128}Xe/^{130}Xe is comparable to (although slightly less than) that of the other samples (Table V). We can also exclude the two-step reaction (α,p) followed by (p,n) because of energetics considerations [27] as well as the lack of sufficient sources of α particles in our samples (Sec. III C 2).

Unlike other cosmic ray components, a significant flux of muons survives at depth, and there is reason to believe that muon reactions may have influenced the excess Xe composition of at least some of our samples. This suggestion is based on our observation of ^{126}Xe excesses of 10^4 atoms/g (4–5 % of the size of the ^{128}Xe excesses) in all of the native Te ores (Table II and Fig. 5). No excesses were observed for the comparably low abundance isotope ^{124}Xe, however. In the deep Kalgoorlie krennerite sample there is again no ^{124}Xe excess, but the ^{126}Xe excess is substantially smaller than in the native Te. The comparatively large uncertainties in the excess ^{124}Xe and ^{126}Xe abundances for the altaite sample preclude comparison with the native Te or Kalgoorlie krennerite. Similar to the case for ^{128}Xe, the excesses of ^{126}Xe in the native Te ores correlate with excess ^{130}Xe from $\beta\beta$ decay of ^{130}Te, as shown in Fig. 6. However, the ^{124}Xe/^{132}Xe ratio remains at the air Xe value in all extraction steps. These observations rule out the possibility that the excess ^{126}Xe is an experimental artifact due, for example, to improper correction for instrumental mass discrimination or to some isobaric interference at mass 126 unrelated to Te. We therefore conclude that the excess ^{126}Xe is derived from Te and is the product of some nuclear transmutation.

The absence of ^{124}Xe excesses coupled with the presence of ^{126}Xe excesses suggests the role of iodine isobar production channels, since production of ^{124}Xe is blocked by positron decay of ^{124}I, but production of ^{126}Xe can occur via decay of ^{126}I. We can exclude neutron, α-capture, and cosmic ray spallation reactions as sources of the ^{126}Xe excesses by the same lines of reasoning that led us to conclude that these processes could not account for the excess ^{128}Xe. Haxton [27] has suggested that charged-current solar neutrino reactions with ^{126}Te can produce excess ^{126}Xe. However, we calculate that such interactions would produce far too little ^{126}Xe (by a factor of about 80) to account for the observed excesses of

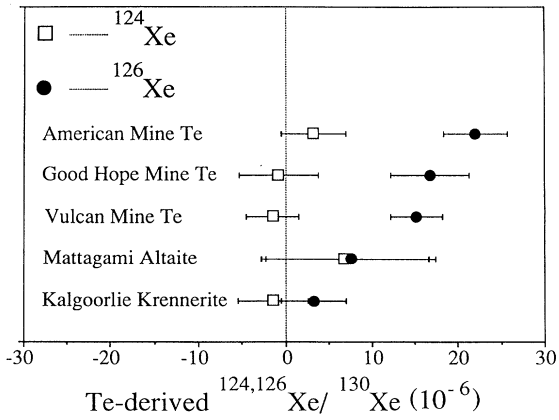

FIG. 5. Total excesses of ^{124}Xe and ^{126}Xe relative to trapped atmospheric Xe in Te ores, normalized to ^{130}Xe from $\beta\beta$ decay of ^{130}Te. No excesses of ^{124}Xe are evident in any sample, but small excesses of ^{126}Xe are present in the native Te samples. See text for discussion.

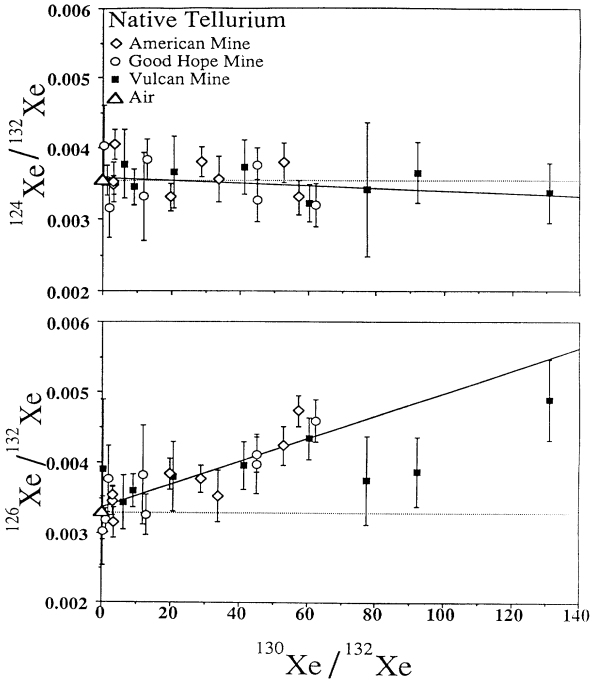

FIG. 6. Correlations of ^{124}Xe and ^{126}Xe with ^{130}Xe in vacuum crushing and stepwise heating of Colorado native Te ores. Dotted lines represent the atmospheric Xe isotopic ratios and solid lines are least-squares fittings to the data. For ^{124}Xe there are no excesses relative to atmospheric Xe composition, but the ^{126}Xe excesses are correlated with ^{130}Xe from $\beta\beta$ decay of ^{130}Te.

this nuclide in our native Te samples. Two remaining potential mechanisms are direct reactions of energetic muons with ^{126}Te in the native Te itself, and secondary (p,n) reactions from energetic protons produced by muons both in the Te and in surrounding rocks. Both of these mechanisms can produce ^{126}Xe unaccompanied by ^{124}Xe.

For the direct reaction we consider $\mu^{\pm}+{}^{126}\text{Te}\rightarrow\mu^{\pm}+{}^{126}\text{I}+\pi^{-}$ which is then followed (46% of the time) by the reaction $^{126}\text{I}\rightarrow e^{-}+\bar{\nu}+{}^{126}\text{Xe}$. The total cross section for the direct reaction has been estimated by Bezrukov and Bugaev [30] by assuming the vector dominance model as $\sigma\approx 1.5\times 10^{-29}$ cm^2/nucleon and is consistent with that deduced from cosmic ray experiments performed in mines as reviewed by Fowler and Wolfendale [31]. The interactions of muons with ^{126}Te will also produce positive pions (as often as they produce negative pions), and in that case the nucleus will be transformed into ^{126}Sb which will decay back to ^{126}Te. When the muon interacts with ^{126}Te, many nucleons may evaporate away, but among neutron-producing events the 0-neutron escape that leads to ^{126}I production will likely have the largest cross section, which we estimate as 0.1 of the total cross section. For a surface muon fluence of about 0.03 cm^{-2} sec^{-1} we then arrive at a rough estimate of the direct reaction surface production rate of 7×10^4 atom ^{126}Xe/g of Te per 10^6 yr, which is more than adequate to account for the 10^4 atom ^{126}Xe/g observed excesses in the native Te. At more realistic sample recovery depths (for Colorado tellurides) of, say, 10–100 m, the muon flux falls by factors of 8–340, respectively, and exposure times on the order of 1.3×10^6 to 54×10^6 yr are required. These exposure times, particularly at the lower end, are geologically reasonable. Here we have ignored any increase in muon reaction cross section due to the increase hardness of the muon spectrum with depth. As these calculations show, near-surface exposure will dominate the muon production of ^{126}Xe in the Te ore's lifetime because of the rapid decrease of the muon flux with depth.

In estimating the effectiveness of the secondary $^{126}\text{Te}(p,n)^{126}\text{I}$ process, we note that the evaporation prongs from muon reactions will have typical kinetic energies of 100 MeV with ranges of 30 g/cm^2 in rock. On the other hand, the mean free path for nuclear reactions in rock is about 120 g/cm^2, which means that the interaction probability is about 25%. We assume a near-unit probability that in any muon reaction at least one proton will be produced and estimate that one-quarter of the potential interactions involving these protons will be (p,n). These rough estimates lead to an energetic proton cross section for production of ^{126}I via the (p,n) that is 6% of the total muon cross section, compared to the 10% estimated for the 0-neutron direct muon reaction. Thus, we guess that such (p,n) reactions will contribute nearly equally in production of ^{126}Xe, which would cut the exposure time estimates given above by somewhat less than half. We will later consider (Sec. IV E) the implications of these calculations for an experiment proposed by Haxton [27] for monitoring the long-term solar neutrino flux using ^{126}Xe from Te ores.

What are the implications for ^{128}Xe production by these muon-related reactions? A naive guess for the production of ^{128}Xe relative to ^{126}Xe is given by assuming equal interaction cross sections per nucleon for ^{128}Te and ^{126}Te. In particular, the production ratio for muon-induced reactions may be estimated as

$$(^{128}\text{Xe}/^{126}\text{Xe})_{\text{muon}}\approx(^{128}\text{Te}/^{126}\text{Te})(\text{B}^{128}/\text{B}^{126})(128/126)\ , \tag{4}$$

where B is the branching ratio for β-decay from iodine ($\text{B}^{128}/\text{B}^{126}=2.04$). The right-hand side of Eq. (4) is 3.47, and the ^{128}Xe/^{130}Xe ratio, corrected for interaction of cosmic ray muons and their secondaries with Te, is thus

$$(^{128}\text{Xe}/^{130}\text{Xe})_{\text{corr}}\approx(^{128}\text{Xe}/^{130}\text{Xe})_{\text{excess}} - 3.47(^{126}\text{Xe}/^{130}\text{Xe})_{\text{excess}}\ , \tag{5}$$

where we have ignored comparable corrections to the ^{130}Xe because of the far greater abundance of this isotope.

In Table V, we illustrate the effect of this correction on the excess ^{128}Xe/^{130}Xe ratios. The greatest reduction in the ^{128}Xe/^{130}Xe ratio is to the native Te samples ($\sim$15%) and the least to the Kalgoorlie krennerite ($\sim$3%). Although it is difficult to make a decisive evaluation of the accuracy of this calculation, we can at least perform some checks on the general consistency of the results. A key sample in this regard is the Kalgoorlie krennerite, which evidently had substantial shielding ($\geq$300 m) for its entire history and consequently was exposed to only a greatly reduced flux of cosmic ray muons ($<2\times 10^{-4}$ of the surface flux). This conjecture is supported by the observation of only a small or nil excess ^{126}Xe/^{130}Xe ratio (Table II) for this ore. Assuming that ^{128}Xe from muon-induced reactions is negligible for the Kalgoorlie krennerite and its excess ^{128}Xe results essentially only from $\beta\beta$ decay, the uncorrected excess ^{128}Xe/^{130}Xe ratio should be close to the true $\beta\beta$-decay production ratio. If the muon-related corrections are valid, the corrected excess ^{128}Xe/^{130}Xe ratios for the other samples should be identical to the uncorrected ratio for the Kalgoorlie krennerite [$(3.38\pm 0.17)\times 10^{-4}$], as is, in fact, observed: the uncorrected Kalgoorlie ratio is in relatively poor agreement with the mean uncorrected ratio for the native Te samples [$(3.85\pm 0.10)\times 10^{-4}$], but in good agreement with the mean ratio for the native Te samples corrected for muon-induced reactions [$(3.26\pm 0.12)\times 10^{-4}$].

Figure 7 is a three-isotope correlation diagram similar to Fig. 4 (see discussion in Sec. III C) in which we show the results of correcting the ^{128}Xe data of individual Xe extraction steps of all samples (except Cripple Creek) for cosmic ray muon interactions, based on the amount of excess ^{126}Xe released in each step. In this three-isotope correlation diagram, ^{132}Xe has also been corrected for small fission Xe contributions according to the procedures detailed in Sec. III A. The entire data set forms a self-consistent linear array (reduced $\chi^2=1.04$, with the number of degrees of freedom of 44) representing a mixture of trapped atmospheric Xe and Xe derived from $\beta\beta$ decay of Te. The slope of this line is identical to the

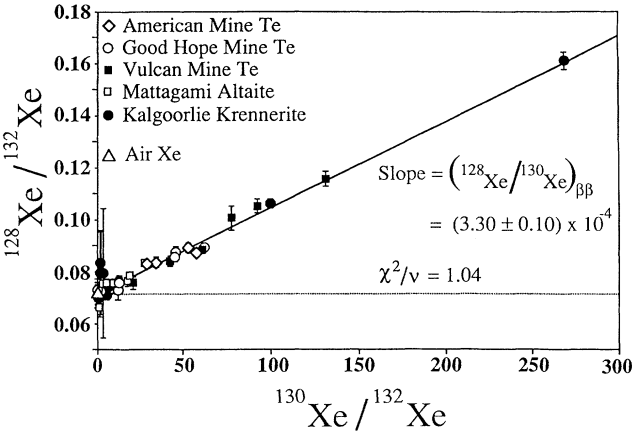

FIG. 7. Correlation of ^{128}Xe with ^{130}Xe from $\beta\beta$ decay in vacuum crushing and stepwise heating data from old Te ores. The ^{128}Xe data have been corrected for muon-induced ^{128}Xe production, and the ^{132}Xe data have been corrected for minor amounts of fission Xe. The slope of the correlation line thus gives the ratio of ^{128}Xe to ^{130}Xe production in $\beta\beta$ decay of Te. See text for discussion.

mean of the muon-corrected ratios in Table V, both giving $(^{128}Xe/^{130}Xe)_{\beta\beta}=(3.30\pm0.10)\times10^{-4}$. We take this value as the most precise and accurate determination of the relative Xe production from $\beta\beta$ decay.

Because of the extremely long decay lifetimes for Te $\beta\beta$ decay, the abundances of the Xe daughters depend linearly on the sample age, and thus the ratio of half-lives is independent of sample age and is related to the $^{128}Xe/^{130}Xe$ ratio by

$$T^{130}_{1/2}/T^{128}_{1/2}=\Gamma^{128}/\Gamma^{130}$$
$$=(^{128}Xe/^{130}Xe)_{\beta\beta}(^{130}Te/^{128}Te)\ . \qquad (6)$$

Using the best estimate of the $^{128}Xe/^{130}Xe$ ratio for Te $\beta\beta$ decay given above and with $^{130}Te/^{128}Te=1.0666$, we arrive at our final result (Table V) for the ratio of Te $\beta\beta$-decay half-lives, $T^{130}_{1/2}/T^{128}_{1/2}=(3.52\pm0.11)\times10^{-4}$.

D. Geochronology and absolute $\beta\beta$-decay rates

The ratio of decay rates $\Gamma^{128}/\Gamma^{130}$ is established essentially by Xe isotopic measurements alone. On the other hand, the absolute decay rate Γ^{130} is found from

$$\Gamma^{130}=(^{130}Xe^*/^{130}Te)/t\ , \qquad (7)$$

where t is the age of the ore, specifically the length of time the ore has retained ^{130}Xe generated *in situ* (hereafter denoted $^{130}Xe^*$). Because radiogenic additions to ^{130}Xe from $\beta\beta$ decay are far more prominent than those to ^{128}Xe and thus subject to less analytical uncertainty, and because $\Gamma^{128}/\Gamma^{130}$ is determined precisely by mass spectrometry from $^{128}Xe/^{130}Xe$ [Eq. (6)], Γ^{128} may be determined to an accuracy comparable to that for $\Gamma^{130}$from the relation $\Gamma^{128}=\Gamma^{130}(\Gamma^{128}/\Gamma^{130})$.

The numerator in Eq. (7) involves measurement of absolute element concentrations and is subject to different uncertainties than an isotopic ratio. Measurement of Te concentration can be made by a variety of techniques that, in principle, have analytical error limits small enough to be inconsequential in the present context. In this and in several prior studies, the $\beta\beta$-decay contribution to the total measured ^{130}Xe is so dominant that the uncertainty in the concentration of $^{130}Xe^*$ is essentially the uncertainty in instrumental sensitivity. This is typically reported, perhaps overoptimistically, as around 10% or better, so that the measurement of $^{130}Xe^*/^{130}Te$ can be conservatively expected to be better than about 20%.

In contrast, calculated decay lifetimes based on a number of Te ores of various ages and geological environments span more than an order of magnitude, and even current "best estimates" for the half-life of ^{130}Te (Sec. IV A) span a factor of 3. The difficulty arises not in the determination of $^{130}Xe^*/^{130}Te$ but in assessing the Xe retention age of the ores. We discuss elsewhere [28] the details of the half-life problem and the relevance of the present data to this problem; a brief summary is given here.

One approach to the problem is to base ^{130}Te half-life estimates only on ores for which there are noble-gas retention ages (K-Ar, U-Xe) for the ores themselves. Few such ages are available. Kirsten [32] stresses the Good Hope (K-Ar age=1.31 Ga [14]) and Boliden (U-Xe age=1.56 Ga [21]) ore ages (1 Ga=10^9 yr), arriving at a best-estimate half-life of $(2.55\pm0.25)\times10^{21}$ yr. A second approach is based on the principle that the age of Xe retention in an ore cannot be greater than the age of mineralization or the age of the host rock. Such an upper limit age provides an upper limit to the decay lifetime, and the lowest such upper bound is thus an upper limit to the true half-life. By this argument Manuel [33] concludes that the half-life of ^{130}Te is no more than 0.8×10^{21} yr. We note that even this lower recommended half-life is about an order of magnitude greater than theoretical expectations (see Sec. IV). We consider that, while both of these approaches are logically sound in principle, both are flawed in terms of practical application to the present problem.

The problem with basing half-life estimates only on ages measured for the ores themselves, by the usual radiogenic daughter accumulation methods, is that the radioactive parent elements on which such methods are based (e.g., K, U, Rb, Sm) are generally of very low abundance in Te ores. Besides potential complications in measuring very low elemental abundances by conventional analytical techniques, this circumstance increases the likelihood that the inventory of the parent element is dominated by trace or accessory mineral phases other than the Te-bearing mineral itself, aggravating problems which can arise in sample heterogeniety and possibly yielding ages which, even if valid for the accessory minerals, are not necessarily applicable to the Te-bearing minerals themselves [34]. The correspondingly low abundance of daughter elements also increases the likelihood that the inventory of the daughter will be substantially affected by inheritance from precursor material or contamination from country rock in which the parent and daughter are more abundant. This is a well-known effect for Ar and He in young igneous rocks [35], and is a plau-

sibly significant effect for the Good Hope samples [34]; similarly, we have already concluded (Sec. III A) that this effect arises for the fission Xe in some of the samples studied here, in that the fission Xe concentrations are too large to be supported by the measured U concentrations (Table IV) for any plausible ore age.

Inheritance of daughter element from precursor material also provides a potential loophole for the second argument described above. Specifically, it is possible that some radiogenic ^{130}Xe may get incorporated into Te ores at the time of mineralization. If so, the measured ^{130}Xe will be higher than that actually produced by *in situ* $\beta\beta$ decay, leading to an erroneously high ^{130}Te decay rate and a half-life that is too short. It should be noted, however, that rather special circumstances are required for this effect to be significant. Inherited radiogenic Ar, He, and fission Xe can be acquired by ore-depositing hydrothermal fluids from essentially any kind of country rock, and can be prominent in minerals deposited with sufficiently low K and U, but this is not the case for inherited radiogenic ^{130}Xe. Such excesses could only be derived from materials with a previous concentration of Te, i.e., a prior generation of Te ores. We consider it plausible that this phenomenon is relevant to some of the Te ores in the present and previous studies.

Accepting at least for the sake of argument the possibility of inherited radiogenic ^{130}Xe, the methods previously employed in assessing Te ore ages and the half-life of ^{130}Te are suggestive but not constraining, and we must seek other criteria. Besides the Xe data we thus also consider the "common Pb ages" determined from isotopic analysis of Pb in our ores (Table VI). A common Pb age is *not* a radiogenic daughter accumulation age analogous to, e.g., K-Ar or U-Xe ages. It results, rather, from a model [36] for the temporal evolution of average terrestrial Pb isotopic composition from primitive to modern values, and it is applicable to samples of Pb whose isotopic evolution is arrested by being sequestered in materials of very *low* U/Pb ratio, such as the Te ores studied here (Table IV). It is difficult to assign errors to common Pb ages, since variations arise in geological behavior rather than analytical uncertainty; qualitatively, we expect that for samples derived from the Earth's mantle, the common Pb age would be within 0.1 Ga of the true age.

It is relevant that the Vulcan, Good Hope, and Mattagami ores are from so-called "volcanogenic massive sulfide deposits" [13,37]. These deposits are believed to have formed from hydrothermal circulation associated with oceanic spreading-center volcanism. This feature is particularly important in the present context because in such deposits both the Te and Pb are expected to be *juvenile* materials extracted from the Earth's mantle (without the potential complication of passage through the continental crust)—the situation for which common Pb model ages are most applicable and for which inheritance of radiogenic ^{130}Xe from any preexisting Te concentration is unlikely.

The Vulcan and Good Hope ores have very similar ^{130}Xe*/Te ratios (Table IV), which are also quite similar to those from previous analyses [9,14,38] of Good Hope native Te [the total range in ^{130}Xe*/Te is $(2.1-2.8)\times10^{-11}$ cm^3 STP/g]. They also have essentially indistinguishable common Pb ages (Table VI), and it is thus difficult to avoid the conclusion that these ores have essentially the same age, specifically the same Xe retention age. Discounting the reported K-Ar age [14] for the reasons outlined above, the best available estimate for the age of the native Te ores is the common Pb age of 1.6 Ga. This is much greater than the Tertiary (i.e., $\leq 60\times10^6$ yr) age commonly associated with telluride mineralization in Colorado (e.g., the Cripple Creek samples, cf. Table VI), but these mines are not associated with Tertiary volcanism [13] and the common Pb age is consistent with that of the host rocks (1.76 Ga) for these deposits [39].

Our result for ^{130}Xe*/Te in Mattagami altaite is consistent with prior data [8,38,40], and our common Pb age (2.67 Ga) is consistent with the age (2.72 Ga) of the host Abitibi greenstone belt [41]. The corresponding inferred half-life of ^{130}Te for Mattagami is also in agreement with that determined for the Vulcan and Good Hope native Te ores (Table VI).

The Colorado Cripple Creek deposit is also associated with volcanic activity, but with young (Tertiary) volcanics erupting through older (Precambrian) continental crust [20]. For its age, this deposit has relatively high ^{130}Xe*/Te that may result from inheritance of ^{130}Xe from older Te ores. Such a scenario is plausible, since a much older generation of Te ores is demonstrably present in the same geographical region, as evidenced by the 1.6 Ga common Pb ages of our Colorado native Te samples.

TABLE VI. Sample ages and Te $\beta\beta$-decay half-lives.

Sample	Common Pb age (10^9 yr)[a]	$T_{1/2}(130)$ (10^{21} yr)	$T_{1/2}(128)$ (10^{24} yr)
Native Te (American Mine, CO)	1.66	3.24	9.22
Native Te (Good Hope Mine, CO)	1.60	2.82	7.99
Native Te (Vulcan Mine, CO)	1.61	2.79	7.92
Altaite: $PbTe_2$ (Mattagami Lake, Quebec)	2.67	2.58	7.32
Krennerite: $(Au,Ag)Te_2$ (Kalgoorlie, Australia)	0.75	0.33	0.94
Krennerite: $(Au,Ag)Te_2$ (Cripple Creek, CO)	(0.028)[d]	0.94	
Calaverite: $AuTe_2$ (Cripple Creek, CO)	(0.028)[d]	0.91	
Mean value		2.73[b] $\pm$0.13	7.74[c] $\pm$0.37

[a]Computed using the two-stage Stacey-Kramers [36] common Pb evolution model.

[b]Based on data for Good Hope and Vulcan native Te and Mattagami altaite. Stated uncertainty is for 1σ dispersion about the mean.

[c]Computed from $T_{1/2}(130)$ for Good Hope and Vulcan native Te and Mattagami altaite using mean half-life ratio given in Table V (column 4). See text for discussion.

[d]Stated age is geological age [20]. Common Pb in these samples is modern, but the method cannot resolve such small ages.

The American Mine and Kalgoorlie deposits are not directly associated with igneous activity but rather with tectonic shearing of crustal igneous intrusions [42]. Mineralization at the American Mine deposit evidently occurred shortly after formation of its host rock, as evidenced by comparison of its 1.66 Ga common Pb age with the age [43] of the host rock (1.67–1.71 Ga). Both the age and $^{130}Xe^*/Te$ of the American Mine native Te are similar to those of the Good Hope and Vulcan Te (Tables IV and VI). On the somewhat finer scale, however, we note that the Good Hope and Vulcan ores have identical ^{130}Xe concentrations but the American Mine ore has a slightly (10%) lower ^{130}Xe concentration, requiring either that this ore lost 10% of its Xe or that it formed roughly 160×10^6 yr later than the other two. Since geological ore deposition environments change appreciably on this time scale, we think that Xe loss is the more likely possibility.

The gold mineralization age at Kalgoorlie is 2.4 Ga [44], as cited in other Te-Xe studies [6]. While the dated ores are tectonically deformed, however, the Te-rich ores are not [45], and are thus *younger* than 2.4 Ga. Our data independently suggest that the isotopic evolution of Pb was arrested by Te ore formation at a substantially more recent time (Table VI). For its age, the $^{130}Xe^*/Te$ in the Kalgoorlie krennerite is relatively high (Tables IV and VI) and, in general, the $^{130}Xe^*/Te$ ratios in Kalgoorlie tellurides [6,22] are also quite variable $[(4-14)\times10^{-11}$ cm^3 STP/g], spanning a range that is well beyond analytical uncertainties. We consider that these observations point to variable degrees of inheritance of ^{130}Xe from older Te ores.

In light of the above considerations, we take the ores from volcanogenic massive sulfide deposits as the ones likely to provide a reliable determination of the ^{130}Te half-life. The relevant ores from the present study comprise two distinct ore deposits of significantly different ages: the 1.6 Ga Colorado Good Hope and Vulcan native Te ores and the 2.7 Ga Quebec Mattagami altaite. These ores yield a mean ^{130}Te half-life of $(2.7\pm0.1)\times10^{21}$ yr, corresponding to a decay rate $\Gamma^{130}=(2.6\pm0.1)\times10^{-22}$ yr^{-1}. Combining this result with the ratio of decay rates $\Gamma^{128}/\Gamma^{130}=(3.52\pm0.11)\times10^{-4}$ derived above, we obtain a decay rate of $\Gamma^{128}=(9.0\pm0.5)\times10^{-26}$ yr^{-1} and a ^{128}Te half-life of $(7.7\pm0.4)\times10^{24}$ yr (Table VI). The ^{128}Te half-life thus determined represents the longest decay lifetime ever measured.

Because our selection of Te ores suitable for the determination of absolute decay rates is based solely on the criterion that they originate in volcanogenic massive sulfide deposits (for which inheritance of radiogenic ^{130}Xe from any preexisting Te concentration is unlikely), it is instructive to consider collectively *all* of the existing data meeting this one requirement. In addition to the Mattagami, Vulcan, and Good Hope samples from the present experiment, we can include three previous analyses of Mattagami altaite [8,38,40] and three previous analyses of Good Hope native Te [9,14,38] in a "grand mean" ^{130}Te half-life. Assuming the common Pb ages of 1.6 Ga for Good Hope and Vulcan and 2.7 Ga for Mattagami, the result is $(2.5\pm0.4)\times10^{21}$ yr, based on nine separate $^{130}Xe^*/Te$ determinations by three independent laboratories, and is consistent with the value derived from the present data alone. The 1σ dispersion about this mean is 16%, within our estimate of the maximum likely analytical uncertainty (20%) in $^{130}Xe^*/^{130}Te$. The relatively small dispersion in the "grand mean" ^{130}Te half-life justifies the assumption that accidental inheritance of ^{130}Xe is not a problem for these two ore deposits. Moreover, because of the substantial difference in formation age of the deposits ($\Delta t\sim1$ Ga), the coherence of half-lives likewise renders unlikely any significant problem with thermally induced loss of radiogenic ^{130}Xe in *either* deposit.

Despite the generally satisfactory nature of the "grand mean" ^{130}Te half-life, we prefer the absolute half-life determinations based exclusively on the present results for two reasons. First, the absolute Xe abundances derived here were based on two independent volumetric calibrations, with an *absolute* uncertainty ($<5\%$) which is generally better than in previous determinations. Secondly, the Te concentrations previously reported for some of the ore samples included in the "grand mean" are almost certainly underestimated. For example, Richardson *et al.* [38] analyzed a sample of "essentially pure Te" taken from the same parent specimen as that of the Good Hope Mine sample investigated by Kirsten, Richter, and Jessberger (who reported 100 ± 0.6 % Te [9], consistent with our analysis) but measured its Te concentration as only 90.3%. Similarly, Lee, Manuel, and Thorpe [8] report Te concentrations for Mattagami altaite and Kalgoorlie krennerite from atomic absorption analysis that are systematically low (5–20 %) compared to both the values determined by EDS in the present work (Sec. II) and values reported in the literature based on wet chemical analysis [15]. Since the absolute half-life of ^{130}Te is proportional to the $Te/^{130}Xe^*$ ratio, the effect of these underestimates of Te concentration is to underestimate the ^{130}Te half-life. Because of these problems, we regard the ^{130}Te half-life of $(2.7\pm0.1)\times10^{21}$ yr determined from the present data as the best value currently available.

IV. DISCUSSION

In the present study the $\beta\beta$ decay of ^{128}Te has been firmly established and the previous conflict regarding its observation has been resolved. The principal results are a precise and accurate determination of the relative ^{128}Te and ^{130}Te $\beta\beta$-decay rates and an improved measurement of the absolute rates. In the following discussion, we note the implications of these results for several topics, including the Majorana mass of the neutrino, limits on the strength of right-handed weak interactions, and bounds on decay rates for 0ν $\beta\beta$-decay accompanied by emission of a Majoron. A summary of these points has been presented in a previous paper [56].

A. Comparison with theoretical decay rates

Prior to the present work, several "best estimates" for the half-life of ^{130}Te have been given in the literature,

based on compilations of previous analyses. Manuel [33] has recommended a value of 8×10^{20} yr, while Kirsten *et al.* [10] have given conservative limits of $(1.5-2.75)\times10^{21}$ yr based only on ores which have been internally dated. We have already pointed out the likely causes (Sec. III D) of the scatter of results in previous half-life determinations; nevertheless, both of these estimates correspond to decay rates considerably slower, typically by 1–2 orders of magnitude, than those in practically all theoretical computations [12,46–50]. Our result of $(2.7\pm0.1)\times10^{21}$ yr is consistent with the Kirsten *et al.* limits, and in our view is sufficiently robust that experimental problems cannot be invoked to account for the divergence between prediction and observation. There is thus a real suppression of the ^{130}Te 2ν decay rate which is not adequately dealt with in $\beta\beta$-decay theories. The present work extends this conclusion to ^{128}Te as well, since the observed ^{128}Te half-life of $(7.7\pm0.4)\times10^{24}$ yr is similarly suppressed relative to the theoretical predictions.

As discussed in the Introduction, the decay of ^{130}Te is dominated by the two-neutrino decay mode [Eq. (1)], while other decay modes [e.g., Eq. (2)] may possibly contribute to the total decay width $\Gamma^{128}_{\text{total}}$ of ^{128}Te. The inadequacy of theory in duplicating the observed 2ν decay rate for ^{130}Te strongly suggests that comparison of *absolute* theoretical and observed 2ν $\beta\beta$-decay rates of heavy nuclei cannot yet be profitably used as reliable indicators of the rates of these other $\beta\beta$-decay modes.

B. Limits on the 0ν decay rate

Despite the inaccuracy of the absolute 2ν decay rate calculations implied by comparison of theory with the present experimental results, most $\beta\beta$-decay models predict a *ratio* of 2ν decay widths, $\rho_{2\nu}=\Gamma^{128}_{2\nu}/\Gamma^{130}_{2\nu}$, which is in fair agreement with observation. In particular, these models [11] give $\rho_{2\nu}\geq2\times10^{-4}$, compared to our result $\rho_{\text{total}}=(3.52\pm0.11)\times10^{-4}$. While it is tempting to ascribe any difference between the total decay ratio and the predicted 2ν decay ratio to the presence of neutrinoless channels in ^{128}Te decay, we resist doing so because the theoretical calculations generally overestimate the 2ν matrix elements for both ^{128}Te and ^{130}Te by large factors, with widely varying results. However, most calculations of the 0ν matrix elements are in fair agreement, at least on a factor of 2 level, and we thus can have better confidence in using the measured ^{128}Te decay rate *alone* to set limits on the neutrinoless decay rate. The problem with this approach is partly experimental, in that this rate is known with considerably less precision (because of the reliance on measurements of absolute Xe concentration) and less accuracy (because of systematic uncertainties in Te ore ages and Xe concentrations; Sec. III D) than the ratio of decay rates. With this caveat in mind, we conservatively take the total decay width $\Gamma^{128}_{\text{total}}=(9.0\pm0.5)\times10^{-26}$ yr^{-1} as an upper bound on the 0ν decay width:

$$\Gamma^{128}_{0\nu}\leq\Gamma^{128}_{\text{total}}\ , \tag{8}$$

whence a lower limit on the half-life for 0ν decay of ^{128}Te is given by the experimentally determined ^{128}Te half-life,

$$(T^{128}_{1/2})_{0\nu}\geq(7.7\pm0.4)\times10^{24}\text{ yr}\ . \tag{9}$$

C. Majorana neutrino mass and right-handed currents

In theoretical calculations of 0ν $\beta\beta$-decay [46–50], the relationship between the decay half-life and neutrino mass is usually presented in the form

$$[(T^{128}_{1/2})_{0\nu}]^{-1}=C_{mm}\langle m\rangle^2+C_{m\eta}\langle m\rangle\langle\eta\rangle+C_{\eta\eta}\langle\eta\rangle^2+\cdots\ , \tag{10}$$

where $\langle m\rangle$ is the effective Majorana mass of the neutrino and $\langle\eta\rangle$ the parameter which scales with the assumed strength of the right-handed weak leptonic currents. The coefficients C are tabulated by various authors. Using the lower limit on the neutrinoless decay half-life [Eq. (9)] and neglecting right-handed currents, we obtain (Table VII) a range of upper limits on the effective Majorana neutrino mass with Eq. (10), from <1.1 to <1.5 eV for various estimates of C_{mm}. We also derive the limit $|\langle\eta\rangle|<5.3\times10^{-8}$ on the basis of coefficients calculated by Suhonen, Khadkikar, and Faessler [50], which give the least restrictive of the estimates. These limits are comparable to the best currently obtained from direct neutrinoless $\beta\beta$-decay searches.

D. Limits on Majoron coupling

We may also use our results to constrain the possibility of neutrinoless $\beta\beta$ decay associated with emission of a Majoron [Eq. (3)]. The conventional Majoron emission is ruled out at levels far beyond the present sensitivity because of the CERN LEP measurements of the Z^0 decay width [51]. Nonetheless, unconventional Majorons have been postulated that would evade the LEP limits but still contribute to $\beta\beta$ decay. To illustrate the sensitivity of our determination of the ^{128}Te half-life to three-body decays, we apply Eq. (9) to a derivation [52] of the conventional Majoron coupling constant $|\langle g_B\rangle|$ to obtain the limit

$$|\langle g_B\rangle|<3\times10^{-5}\ . \tag{11}$$

A coupling at this limit would then generate the following rates in other $\beta\beta$-decay nuclei:

$$\begin{aligned}
&T_{1/2}(^{48}\text{Ca})>3.8\times10^{23}\text{ yr}\ ,\\
&T_{1/2}(^{76}\text{Ge})>4.9\times10^{23}\text{ yr}\ ,\\
&T_{1/2}(^{82}\text{Se})>7.1\times10^{22}\text{ yr}\ ,\\
&T_{1/2}(^{100}\text{Mo})>3.7\times10^{21}\text{ yr}\ ,\\
&T_{1/2}(^{150}\text{Nd})>2.1\times10^{21}\text{ yr}\ .
\end{aligned} \tag{12}$$

These bounds are considerably more stringent than those derived from experiments currently being performed [53–55]. Although unconventional Majoron models may involve somewhat different nuclear physics, qualitatively it is clear that the total ^{128}Te decay rate is presently our best constraint on three-body decays.

TABLE VII. Upper limits on the effective Majorana neutrino mass (eV). Derived from observational limit $T^{0\nu}_{1/2} > 7.7 \times 10^{24}$ yr for ^{128}Te $\beta\beta$ decay, with $|\langle \eta \rangle| = 0$.

Theory [Ref.]	Upper limit on $\langle m_\nu \rangle$
Haxton [4][a]	1.1
Tomoda [49]	1.1
Suhonen [50]	1.5

[a]Calculated with $g_A/g_V = 1.0$.

E. Constraints on solar neutrino detection

The standard solar model predicts that the Sun's photon luminosity should increase monotonically, and that the ^{8}B neutrino flux should increase exponentially with a doubling time of ~ 0.85 Ga. A test of this prediction has been proposed by Haxton [27], who argues that Te ores will accumulate excess ^{126}Xe from the reaction

$$\nu + {}^{126}\mathrm{Te} \rightarrow {}^{126}\mathrm{I} + e^- \quad (2.15\text{-MeV threshold}) \qquad (13)$$

followed by decay of ^{126}I (46% of the time) to ^{126}Xe. As noted earlier (Sec. III C 5) we have observed $\sim 10^4$ atom/g excesses of ^{126}Xe in our native Te ores. However, we calculate that the reaction of Eq. (13) could account for only $\sim 1\%$ of the effect and have postulated that reactions by cosmic ray muons and energetic secondary protons generated by muon reactions are probably responsible for the observed ^{126}Xe excesses.

Although our experiments were not designed to specifically test the Haxton hypothesis, they do put some additional limitations beyond those already discussed by him [27]. In particular, we calculate that the muon contribution to ^{126}Xe will exceed that from solar neutrinos up to a depth of ~ 2.8 km w.e. (~ 0.4 km of rock $= 1$ km w.e.). The muon contribution drops to 10% of the solar neutrino production at 4.4 km w.e. (roughly the depth of the Homestake Mine), and neglecting other difficulties, candidate samples from this or greater depth could be used. We note in passing, however, that even with the high-sensitivity instrument used in the present experiment, it would require a kg-sized Te sample with trapped Xe concentrations comparable to those in the present experiment to obtain an uncertainty level of 50% in the excess ^{126}Xe abundance due simply to counting statistics.

ACKNOWLEDGMENTS

We thank O. K. Manuel of the University of Missouri at Rolla for samples of altaite and krennerite, P. Dunn of the National Museum of Natural History for the native Te samples, and R. Grauch of the U. S. Geological Survey in Denver for the Cripple Creek tellurides. C. Alexander provided many useful suggestions. We are happy to acknowledge the guidance and support of R. M. Walker of the McDonnell Center for the Space Sciences, and we are particularly grateful to W. C. Haxton of the University of Washington at Seattle for many discussions of the theoretical aspects of $\beta\beta$ decay.

[1] See reviews by F. T. Avignone III and R. L. Brodzinski, in *Neutrinos,* edited by H. V. Klapdor (Springer-Verlag, New York, 1988), p. 147; K. Muto and H. V. Klapdor, *ibid.* p. 183; M. Doi, T. Kotani, and E. Takasugi, Prog. Theor. Phys. Suppl. **83**, 1 (1985); T. Tomoda, Rep. Prog. Phys. **54**, 53 (1991). See also Ref. [4].

[2] B. Kayser, *The Physics of Massive Neutrinos* (World Scientific, Singapore, 1989), p. 72.

[3] M. G. Inghram and J. H. Reynolds, Phys. Rev. **76**, 1265 (1949); **78**, 822 (1950).

[4] W. C. Haxton and G. J. Stephenson, Prog. Part. Nucl. Phys. **12**, 409 (1984).

[5] H. Primakoff and S. P. Rosen, Rep. Prog. Phys. **22**, 121 (1959); Proc. Phys. Soc. **78**, 464 (1961).

[6] E. W. Hennecke, O. K. Manuel, and D. D. Sabu, Phys. Rev. C **11**, 1378 (1975).

[7] E. W. Hennecke, Phys. Rev. C **17**, 1168 (1978).

[8] J. T. Lee, O. K. Manuel, and R. I. Thorpe, Nucl. Phys. **A529**, 29 (1991).

[9] T. Kirsten, H. Richter, and E. Jessberger, Phys. Rev. Lett. **50**, 474 (1983).

[10] T. Kirsten *et al.*, in *Nuclear Beta Decays and Neutrino,* edited by T. Kotani, H. Ejiri, and E. Takasugi (World Scientific, Singapore, 1986), p. 81.

[11] See, e.g., Table 5.2 in K. Muto and H. V. Klapdor, *Neutrinos,* Ref. [1].

[12] A. G. Williams and W. C. Haxton, in *Intersections Between Particle and Nuclear Physics,* Proceedings of a Conference held in Rockport, ME, 1988, edited by R. Lerner, AIP Conf. Proc. No. 176 (AIP, New York, 1988), p. 924.

[13] P. D. Hartley, *Gunnison Gold Belt and Powderhorn Carbonatite Field Trip Guidebook* (Denver Region Exploration Geologists Society, Denver, 1983), p. 19.

[14] T. Kirsten *et al.*, Phys. Rev. Lett. **20**, 1300 (1968).

[15] N. D. Sindeeva, *Mineralogy and Types of Deposits of Selenium and Tellurium* (Interscience, New York, 1964).

[16] S. Niemeyer and D. Leich, in *Proc. Lunar Sci. Conf. 7th* (Pergamon, New York, 1976), Vol. 1, p. 587.

[17] C. M. Hohenberg, Rev. Sci. Instrum. **51**, 1075 (1980).

[18] J. C. Brannon *et al.*, Geochim. Cosmochim. Acta **55**, 1407 (1991).

[19] G. B. Hudson, Ph.D. thesis, Washington University, 1981.

[20] T. B. Thompson, A. D. Trippel, and P. C. Dwelley, Econ. Geol. **80**, 1669 (1985).

[21] T. Kirsten, W. Gentner, and O. Müller, Z. Naturforsch. Teil A **22**, 1783 (1967).

[22] B. Srinivasan, E. C. Alexander, and O. K. Manuel, J. Inorgan. Nucl. Chem. **34**, 2381 (1972).

[23] J. C. Browne and B. L. Berman, Phys. Rev. C **8**, 2405 (1973).

[24] D. J. Hughes and R. B. Schwartz, *Neutron Cross Sections* (Brookhaven National Laboratory, New York, 1958).

[25] W. C. Haxton (private communication).

[26] G. Bozoki and K. Lande, Il Nuovo Cimento **12B**, 65 (1972).

[27] W. C. Haxton, Phys. Rev. Lett. **65**, 809 (1990).

[28] J. C. Brannon *et al.*, Geochim. Cosmochim. Acta (to be published).

[29] O. K. Manuel (private communication).

[30] L. B. Bezrukov and E. V. Bugaev, in *Proceedings of 17th International Cosmic Ray Conference* (International Union of Pure and Applied Physics, France, 1981), Vol. 7, p. 90.
[31] G. N. Fowler and A. W. Wolfendale, Prog. Elem. Part. Cosmic Ray Phys. **IV**, 107 (1958).
[32] T. Kirsten, in *Science Underground (Los Alamos National Laboratory, New Mexico),* Proceedings of a Workshop on Science Underground, edited by M. M. Nieto, W. C. Haxton, C. M. Hoffman, E. W. Kolb, V. D. Sandberg, and J. W. Toers, AIP Conf. Proc. No. 96 (AIP, New York, 1982), p. 396.
[33] O. K. Manuel, J. Phys. G **17**, S221 (1991).
[34] J. T. Lee and O. K. Manuel (submitted to Earth Planet. Sci. Lett.)
[35] M. Ozima and F. A. Podosek, *Noble Gas Geochemistry* (Cambridge University Press, London, 1983).
[36] J. S. Stacey and J. D. Kramers, Earth Planet. Sci. Lett. **26**, 207 (1975).
[37] J. Luden and C. Hubert, Geology **14**, 707 (1986).
[38] J. F. Richardson *et al.*, Nucl. Phys. **A453**, 26 (1986).
[39] M. E. Bickford *et al.*, Geol. Soc. Am. Spec. Pap. **235**, 33 (1989).
[40] W. J. Lin *et al.*, Nucl. Phys. **A481**, 484 (1988).
[41] T. Krogh, Geochim. Cosmochim. Acta **46**, 637 (1982).
[42] However, many gold tellurides in Boulder Co., CO *are* associated with Tertiary volcanics. See W. C. Kelly and E. N. Goddard, Geol. Soc. Am. Memoir **109** (1969).
[43] W. P. Premo and W. R. van Schmus, Geol. Soc. Am. Spec. Pap. **235**, 13 (1989).
[44] A. G. Mueller *et al.*, Ore Geol. Rev. **3**, 359 (1988).
[45] G. N. Phillips, Econ. Geol. **81**, 779 (1986).
[46] P. Vogel and M. R. Zirnbauer, Phys. Rev. Lett. **57**, 3148 (1986).
[47] K. Grotz and H. V. Klapdor, Nucl. Phys. **A460**, 395 (1986).
[48] K. Muto, in *Proceedings of the International Symposium on Nuclear Beta Decays and Neutrino,* edited by T. Kotani, H. Ejiri, and E. Takasugi (World Scientific, Singapore, 1986), p. 177.
[49] T. Tomoda and A. Faessler, Phys. Lett. B **199**, 475 (1987).
[50] J. Suhonen, S. B. Khadkikar, and A. Faessler, Nucl. Phys. **A535**, 509 (1991).
[51] LEP Collaboration, Phys. Lett. B **276**, 247 (1992); for theoretical motivation, see Georgi *et al.* in Ref. [52].
[52] H. M. Georgi, S. L. Glashow, and S. Nussinov, Nucl. Phys. **B193**, 297 (1981); J. D. Vergados, Phys. Lett. **109B**, 96 (1982); M. Doi, T. Kotani, and E. Takasugi, Phys. Rev. D **37**, 2575 (1988), also Ref. [49]; see K. Muto and H. V. Klapdor, in *Neutrinos,* Ref. [1].
[53] D. O. Caldwell *et al.*, Nucl. Phys. B Proc. Suppl. **13**, 547 (1990); A. S. Starostin, in *Proceedings of the 25th International Conference on High Energy Physics* (World Scientific, Singapore, 1990); H. Ejiri *et al.*, J. Phys. G **13**, 839 (1987); F. T. Avignone III *et al.*, Phys. Lett. B **198**, 253 (1987); P. Fisher *et al.*, *ibid.* **192**, 460 (1987).
[54] M. K. Moe, Am. Phys. Soc. Bull. **37**, 925 (1992); S. R. Elliot, A. A. Hahn, and M. K. Moe, Phys. Rev. Lett. **59**, 2020 (1987).
[55] F. Avignone, Am. Phys. Soc. Bull. **37**, 1024 (1992).
[56] T. Bernatowicz *et al.*, Phys. Rev. Lett. **69**, 2341 (1992).
[57] F. A. Podosek *et al.*, Earth Planet. Sci. Lett. **10**, 199 (1971).
[58] E. K. Hyde, *The Nuclear Properties of the Heavy Elements III* (Dover, New York, 1971).